NASA Contractor Report 3342

Pilot-Aircraft System Response to Wind Shear

Barry S. Turkel and Walter Frost

NASA

NASA Contractor Report 3342

Pilot-Aircraft System Response to Wind Shear

Barry S. Turkel and Walter Frost
FWG Associates, Inc.
Tullahoma, Tennessee

NASA

National Aeronautics
and Space Administration

**Scientific and Technical
Information Branch**

1980

ACKNOWLEDGMENT

TABLE OF CONTENTS

iii

LIST OF ILLUSTRATIONS

NOMENCLATURE

C_D Drag coefficient, $D/(1/2)\rho V_a^2 S$ (dimensionless)

C_{D_o} Drag parameter (zero angle of attack) (dimensionless)

C_{D_α} Drag derivative (rad^{-1})

$C_{D_{\alpha^2}}$ Drag derivative (rad^{-2})

C_L Lift coefficient $L/(1/2)\rho V_a^2 S$ (dimensionless)

C_{L_o} Lift parameter (zero angle of attack) (dimensionless)

C_{L_q} Lift derivative (rad^{-1})

C_{L_α} Lift derivative (rad^{-1})

$C_{L_{\dot\alpha}}$ Lift derivative (rad^{-1})

$C_{L_{\delta_E}}$ Lift derivative (deg^{-1})

C_m Pitching-moment coefficient, $M/(1/2)\rho V_a^2 S\bar{c}$ (dimensionless)

C_{m_o} Pitching-moment parameter (zero angle of attack) (dimensionless)

C_{m_q} Pitching-moment derivative (rad^{-1})

C_{m_α} Pitching-moment derivative (rad^{-1})

$C_{m_{\dot\alpha}}$ Pitching-moment derivative (rad^{-1})

$C_{m_{\delta_E}}$ Pitching-moment derivative (deg^{-1})

$\bar{c}$ Wing mean aerodynamic chord (m)

D Magnitude of aerodynamic drag (N)

F_T Magnitude of thrust (N)

HA   Reference height (m)

I_{yy} Aircraft moment of inertia around y-axis (kg-m^2)

L Magnitude of aerodynamic lift force (N)

L_T Moment arm of thrust vector (m)

m	Aircraft weight (N)
M	Pitching moment (kg m^2/s^2)
q	Pitch angular velocity (rad/sec)
V	Magnitude of aircraft velocity with respect to the ground (m/s)
V_a	Magnitude of airspeed (m/s)
V_{a_0}	Magnitude of initial airspeed (m/s)
x	Horizontal coordinate (m)
z	Vertical coordinate (m)

Greek Symbols

α	Angle of attack between ground velocity vector and aircraft fuselage reference line (FRL) (rad)
α'	Angle of attack between airspeed vector and aircraft FRL (rad)
γ	Flight path angle (rad)
δ	Angle between airspeed vector and ground speed vector (rad)
δ_E	Elevator deflection angle (deg)
δ_T	Angle between thrust vector and aircraft FRL
Δ_h	Glide slope positional error (- aircraft above, + aircraft below) (m)
$\Delta_{\dot{h}}$	Aircraft descent rate error (- slower, + faster) (m/s)
ϵ	Glide slope error angle (rad)
θ_C	Pitch control variable (m rad/sec^2)
ρ	Air density (g/m^3)

Other

| $(\dot{\ })$ | Time derivative |
| $(\ )_0$ | Initial value |

1.0 INTRODUCTION

Encounter with wind shear during approach and takeoff has gained recognition within the past few years as a major hazard to flight safety. Several accidents and near accidents have now been officially attributed to wind shear. There were probably many more prior to instruments and basic knowledge of the atmosphere which made identification of wind shear as a contributing factor possible. These accidents and near accidents have been mistakenly resolved as pilot error. The most notable accident with wind shear as a major cause involved the Eastern 66, Boeing 727, which crashed on approach in a thunderstorm wind environment at John F. Kennedy International Airport on June 24, 1975, resulting in 113 fatalities [1].* A more recent incident took place on August 22, 1979, in Atlanta as Eastern 693, also a Boeing 727, was forced to abort approach and initiate a go-around after a relatively severe loss of altitude and airspeed [2].

Wind shear is a spatial or temporal gradient in wind speed and/or direction. It has many sources in the atmosphere. A common but generally benign example is the logarithmic wind profile associated with boundary layer flow over homogeneous terrain. A vertical shear exists in the longitudinal wind--the wind velocity has some magnitude w_x at height h which decreases logarithmically to zero at the ground. Other sources of shears are cold and warm fronts, thunderstorms, and perturbed flows around obstacles.

To illustrate the effects of wind shear on an aircraft, two simple examples are examined. Since an airplane's flight depends on horizontal airflow (relative airspeed) over its wings to generate lift, any changes in the relative airspeed will alter the balance of forces that keep the aircraft in straight, unaccelerated, level flight. Therefore, a tail wind shearing to a head wind will increase the relative airflow over the

---

*Numbers in brackets correspond to similarly numbered references in the List of References.

wings, increasing the lift force, and causing the aircraft to ride high on the glide slope. In the case of a head wind shearing to a tail wind, the relative airflow over the wings will decrease, the lift will decrease, and the aircraft will fall below the glide slope. This is a particularly hazardous condition since reaction time and engine spool-up time become relatively small as the plane approaches the runway threshold; premature ground impact may result. Escape from this hazardous situation depends on the severity of the wind conditions, the physical and performance characteristics of the aircraft, and the skill, experience, and reaction time of the pilot. If a trained pilot recognizes his decrease in airspeed and deviation below the glide slope, he can apply the necessary thrust and elevator controls to perform a go-around or land the plane safely.

2.0 <u>WIND SHEAR STUDIES</u>

Previous computer simulations of aircraft flight through wind shear
have suggested that the phugoidal oscillations of commercial jetliners
are excited when the wind spectral frequency approaches the phugoidal
frequency.

McCarthy, Blick, and Bensch [3] used aircraft measured thunderstorm
environment winds as input to their numerical aircraft flight simulation
model. They used a two-dimensional linear system of aircraft motion
equations to perform fixed-stick (constant thrust setting and elevator
deflection angle) flight simulations with an aircraft characteristic of
a Boeing 727. The results of the simulations show that horizontal gusts
at approximately the phugoidal frequency are responsible for most of
the flight path deviation and airspeed oscillation. It was also noted
that flight simulations through a wave-form longitudinal wind profile
representative of the winds encountered by Eastern 66 [1] resulted in
poor approaches.

Frost and Crosby [4] numerically simulated fixed-stick and auto-
matic controlled flight of aircraft characteristic of a DC 8, Boeing
747, DHC-6 Otter, and STOL (short takeoff and landing) through thunder-
storm wind fields. They used a nonlinear two-dimensional three-degrees-
of-freedom model. Two-dimensional thunderstorm wind field data were
provided in tabulated format with a computer lookup routine. The
longitudinal and vertical wind component data used in the study were
measured with an instrumented 500 m tower at the National Severe Storms
Laboratory at Norman, Oklahoma. Time history measurements were converted
to a horizontal spatial coordinate grid using Taylor's hypothesis for
use in the computer lookup routine. Frost and Crosby's simulations
revealed highly amplified phugoidal oscillations along flight trajectories
through these storms.

Extensive work was done in simulated automatic controlled flight
through boundary layer shear, perturbed wind fields around buildings,

and thunderstorm gust fronts by Frost and Reddy [5]. A feedback control loop was developed which passes airspeed error, horizontal and vertical acceleration, and pitch command signals through variable gains to drive the throttle and elevator controls. A detailed discussion of this automatic control system appears in Appendix A.

The aforementioned work has established a relationship between aircraft response to longitudinal thunderstorm gusts; however, the fact remains that influence of a human pilot has not been included. The fixed-stick method is not likely to be flown in a thunderstorm environment, whereas the automatic control system is too perfect. To achieve a more realistic simulation, this study examines the response of the pilot-aircraft system to hazardous wind environments.

The work of Frost and Reddy [5] is expanded to include a human pilot as controller. Computer-simulated flight through variable winds measured along typical flight paths is carried out. The wind data were measured along the glide slope with a Doppler radar. Simultaneously, a Queen Air aircraft made controlled approaches along the glide slope. The measurements were carried out as part of the SESAME '79 program, April and June, 1979, in Oklahoma.

The overall objective of the flight experiment program is to test the feasibility of a Doppler radar wind shear warning and detection system. The operational system concept is to aim a 10.2 cm pulsed Doppler radar along the glide slope at commercial airports and thus supply air traffic control personnel with real-time wind information on the approach path. The Doppler radar system is capable of making a complete scan along the glide slope from 3.5 km (minimum range) to 22.5 km (maximum range) and obtain almost instantaneous wind information in 150 m steps. Such a system would be extremely beneficial in detecting hazardous shear conditions for any aircraft landing on a monitored approach path. Air traffic control personnel can monitor worsening wind shear conditions between takeoffs and landings of various aircraft. Also, a real-time spectral analysis can be performed on the Doppler wind data to determine if phugoidal frequency shear waves particularly hazardous to a given aircraft type exist. The phugoid oscillation is discussed in Section 3.0.

4

In order to compare the effects of the Doppler-detected wind fields on aircraft other than a small commuter-type Queen Air aircraft, an aircraft having characteristics of a Boeing 727 was also flown through one of the wind fields. In addition, the aircraft was flown through sinusoidal longitudinal wind waves having a frequency near the phugoid frequency of the aircraft. The wind field was constructed to have a head wind shearing to a tail wind, thus giving an effect similar to flying directly through the downburst region of a thunderstorm cell.

3.0 THE PHUGOID OSCILLATION

An aircraft responds to a longitudinal disturbance with oscillations in speed, vertical height, and pitch rate. The oscillatory motion can be broken down into two components: the short-period oscillation and the long-period phugoid oscillation. The short-period oscillation is heavily damped, and its associated pitch rate changes "wash out" shortly after the disturbance is encountered. The aircraft is then left with a long-period, low-damped phugoid oscillation which produces slow changes of speed and height. This is usually not a serious problem for a pilot to control since the speed and height changes are not severe and the time period is long. It is insidious, however, when the pilot's attention is directed to other factors. Moreover, encounter with a large wavelength longitudinal disturbance (horizontal wind shear) may exaggerate the phugoid mode, causing a control problem for the pilot.

Analysis of the phugoid oscillation assumes small pitch rates, constant angle of attack, negligible drag effects, and a constant sum of potential and kinetic energy. A simple example involves an aircraft encountering a head wind gust. The initial response is an increase in lift, a pitch-up of the nose, and an increase in height; kinetic energy is converted to potential energy, causing the airspeed to drop and the nose to pitch down. Potential energy is converted back to kinetic energy as the plane begins to descend, picking up airspeed until it once more begins to climb. The kinetic energy of descent is converted to potential energy of height. This simple harmonic motion will damp out after some time.

From Dickinson [6] the degree of phugoid damping for a particular aircraft depends on the aerodynamic derivative x_u, which is the rate of change of force in the x-axis (direction of flight) due to changes in forward speed. This is related to the drag characteristics of the aircraft. Also known as the speed damping derivative, x_u is usually negative and proportional to $-C_D$ where C_D is the drag

6

coefficient. If the aircraft is disturbed in such a way as to increase its forward speed, lift will increase as well as drag, which will eventually reduce the speed back to its initial value.

From McCarthy, Blick, and Bensch [3] the exponential phugoid damping period, or the time for the oscillation to decay to 1/e of its initial amplitude, is given by $T = V_{a_0}/g(C_{L_0}/C_{D_0})$ where V_{a_0} is equilibrium airspeed (m/s), g is the gravitational acceleration (m/s^2), and C_{L_0} and C_{D_0} are the lift and drag coefficients for the particular aircraft. Thus, the high approach speed (V_{a_0}) and high lift-to-drag ratios of commercial jet transport aircraft contribute to a large exponential phugoid damping period. This simply means that the phugoid oscillation of a jet transport will not damp out as quickly as that of a smaller aircraft. This adds significance to the observation that smaller aircraft have escaped longitudinal gusts that later caused large commercial aircraft to crash.

7

4.0 THE PILOT MODEL

The pilot models used in the computer-simulated flights are described in this section.

For the preliminary study, a parametric study of pilot performance rating was carried out. The pilot performance rating model was incorporated into the control loop of Frost and Reddy [5] in the following manner. The automatic feedback control system as described in Appendix A evaluates the difference between the actual and desired state of the simulated aircraft on approach. The system monitors airspeed, horizontal ground speed, vertical velocity, flight path angle deviation and displacement from the glide slope and processes these parameters through variable gains to determine the necessary signals to the throttle and elevator servos. The servos adjust thrust and elevator angle to bring the aircraft back to the desired state. A pilot, who is assumed to be monitoring these same parameters at the same rate as the autopilot, would not be able to respond as fast as the autopilot to the information he receives. Thus, the pilot would not move the servos to correct the plane's deviations as efficiently as the autopilot. In effect, the pilot is always lagging the autopilot. Thus, the pilot's control signal inputs are reduced by a performance rating or "perfection percentage" gain where

8
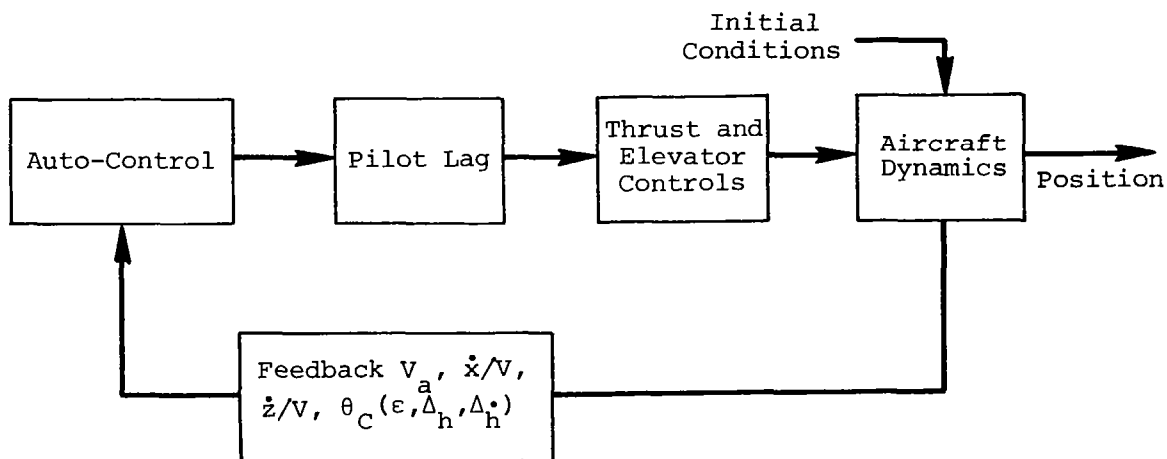
0 percent corresponds to zero inputs (fixed-stick) and 100 percent corresponds to "perfect" autopilot control. This is accomplished in the program by use of the difference equation

$$y_n = y_{n-1} - (y_{n-1} - x_n)k$$

where y_n and y_{n-1} are the control signal outputs for the present and previous time steps, respectively, x_n is the input control signal for the present time step, and k is the "perfection percentage" gain. The pilot constantly attempts to return the aircraft to the desired state, but this occurs at a slower response rate than the "perfect" automatic control system.

'Classifying pilot response by means of a performance rating encompasses the many intangibles encountered in pilot modeling which are too complex to simulate. These intangibles include pilot personality, training, knowledge and warning of the encountered wind shear, as well as the element of surprise. Hence, a pilot with a low performance rating (for example, 0.03, which corresponds to a minimal control input) may be classified as poorly trained, slow-to-react, unknowledgeable, or uninformed of the imminent wind shear. Clearly, more work needs to be done on pilot modeling specifically to determine pilot response to the wind shear environment. However for purposes of this study, the proposed pilot's "perfection percentage" gain gives useful results.

In addition, two runs were carried out using human pilot transfer function data taken during simulator experiments by Adams and Bergeron [7]. They tested six pilots (ages 30 through 47) and two test engineers in a flight simulator equipped with an oscilloscope and control stick. Pilot workload was created by filtering computer-generated noise to obtain a simulated flight disturbance. While viewing the disturbances on the oscilloscope, the subjects were instructed to keep the oscilloscope signal aligned with a marked reference point by moving the control stick. Adams and Bergeron measured the subjects' static gains, lead and lag time constants throughout the runs, examining variations between the subjects for given controlled dynamics (degree of vehicle controllability). The general form of the human pilot transfer function is

9

$$\frac{\delta}{D} = \frac{k_1 \tau \left[1 + \frac{k_2}{\tau} s \right]}{(\tau + s)^2}$$

where

   δ = analog pilot output produced by moving the control stick (volts)

   D = input disturbance sensed visually by the pilot (volts)

   τ = lag time constant (sec^{-1})

k_1/τ = static gain (volts/volts), k_1 units are volts/(volts)(sec)

k_2/τ = lead time constant (sec), k_2 is dimensionless

   s = Laplace operator (sec^{-1})

This transfer function is useful for describing a pilot in a linear single-axis attitude control system in a compensatory tracking task (i.e., glide slope tracking) and provides a representative model for analysis purposes.

Throughout the runs Adams and Bergeron [7] noted that k_1, k_2, and τ stabilized within 30 seconds to near constant values for the remainder of the run. Thus, k_1, k_2, and τ form a constant gains transfer function representative of a given pilot for a given run with specified controlled dynamics. A sample transfer function for pilot F (Table 1), assuming control dynamics = 1 (easily maneuverable and controllable aircraft), with k_1 = 3 volts/(volts)(sec), $k_2 \approx 1$, and τ = 4 sec^{-1} is

$$\frac{\delta}{D} = \frac{0.75[1 + 0.25(s)]}{[1 + 0.25(s)]^2}$$

The complete pilot-aircraft system response to a disturbance (in this case wind shear) is obtained by multiplying the pilot transfer function by the controlled system transfer function. For example, from Adams and Bergeron [7], multiplying the pilot transfer function

$$\frac{\delta}{D} = \frac{k_1 \tau \left[1 + \frac{k_2}{\tau} s \right]}{(\tau + s)^2}$$

and control system dynamics

$$\frac{\theta}{\delta} = 1$$

TABLE 1. Transfer Function Data of the Eight Pilots Investigated in Reference [7].

Controlled System Dynamics	Pilot Identifier	k_1 $\dfrac{\text{volts}}{(\text{volts})(\text{sec})}$	$\cdot\tau$ sec^{-1}	k_2 (dimensionless)
1	A	8.0	8.0	0.0
1	B	6.5	7.0	0.0
1	C	9.0	11.0	0.0
1	D	5.0	5.5	0.5
1	E	9.0	10.0	0.0
1	F	3.0	4.0	1.0
1	G	5.5	6.0	0.5
1	H	3.0	3.0	1.0

where θ is the aircraft system output response (volts) to pilot output which is input to the system yields

$$\frac{\theta}{D} = \frac{\delta}{D} \times \frac{\theta}{\delta} = \frac{k_1\tau\left(1 + \dfrac{k_2}{\tau}s\right)}{(\tau + s)^2}$$

The general form of the pilot-aircraft transfer function

$$\frac{\theta}{D} = \frac{k_1\tau\left(1 + \dfrac{k_2}{\tau}s\right)}{(\tau + s)^2}$$

can be rewritten as

$$\frac{\theta}{D} = \frac{k_1 k_2\left(\dfrac{\tau}{k_2} + s\right)}{(\tau + s)^2}$$

A transfer function of this form multiplied by a step response, 1/s, can be z-transformed into a difference equation of the form

$$y_n = (C1)y_{n-1} + (C2)y_{n-2} + (D1)x_{n-1} + (D2)x_{n-1}$$

(Neuman and Foster [8]) where y_n is the output signal, y_{n-2} and y_{n-1} are the signal outputs of the last two previous time steps, respectively,

and x_{n-2} and x_{n-1} are the signal inputs of the last two previous time steps, respectively. The constants for this difference equation (Neuman and Foster [8]) are

$$C1 = 2e^{-\tau t}$$

$$C2 = -e^{-2\tau t}$$

$$D1 = \frac{k_1}{\tau} + e^{-\tau t}\left[(k_1 k_2 - k_1)t - \frac{k_1}{\tau}\right]$$

and

$$D2 = \left[\frac{k_1}{\tau}(e^{-\tau t} - 1) - (k_1 k_2 - k_1)t\right]e^{-\tau t}$$

The response time t is set equal to 0.01 corresponding to the sampling interval of the computer program used in the flight simulations.

5.0 RESULTS AND DISCUSSION

Doppler radar-detected glide slope longitudinal wind data for the twelve Queen Air SESAME approaches supplied by McCarthy and Elmore of the University of Oklahoma consisted of three sets of data for each flight. Two sets of data were Eulerian or "frozen" glide slope wind scans taken by the Doppler radar before and after the approach of the Queen Air down the glide slope. The third set of data was obtained with the ground-based Doppler radar sampling the wind just ahead of the aircraft as it flew down the glide slope.

In the following simulations, only the Eulerian data sets are used. The raw Eulerian Doppler wind data were recorded in terms of slant range from the radar location and were then converted by McCarthy and Elmore to time history data by Taylor's hypothesis using the average approach speed of the Queen Air. Thus, 24 cases of time history wind data are available as input to the nonlinear flight simulation program. These cases were initially run in the fixed-stick mode to determine which cases, if any, had any significant wind shear to cause airspeed and flight path deviations. Generally, the wind shear in most cases was not severe enough to cause major deviations, but two cases revealed phugoidal-type oscillations in the aircraft's approach trajectory. One of these cases is selected for detailed examinations where the original fixed-stick trajectory is compared with autopilot- and pilot-controlled trajectories. In addition, the simulated flights of a B727 flown through sinusoidal phugoid frequency longitudinal wind waves of varying amplitude are presented.

5.1 Simulated Queen Air Flight Through Queen Air Flight 17/Run 2 Wind Field

The longitudinal winds measured during the SESAME Queen Air Flight 17/Run 2 are used as input to the flight simulation program. Figure 1 shows the head winds encountered during the flight as a function of
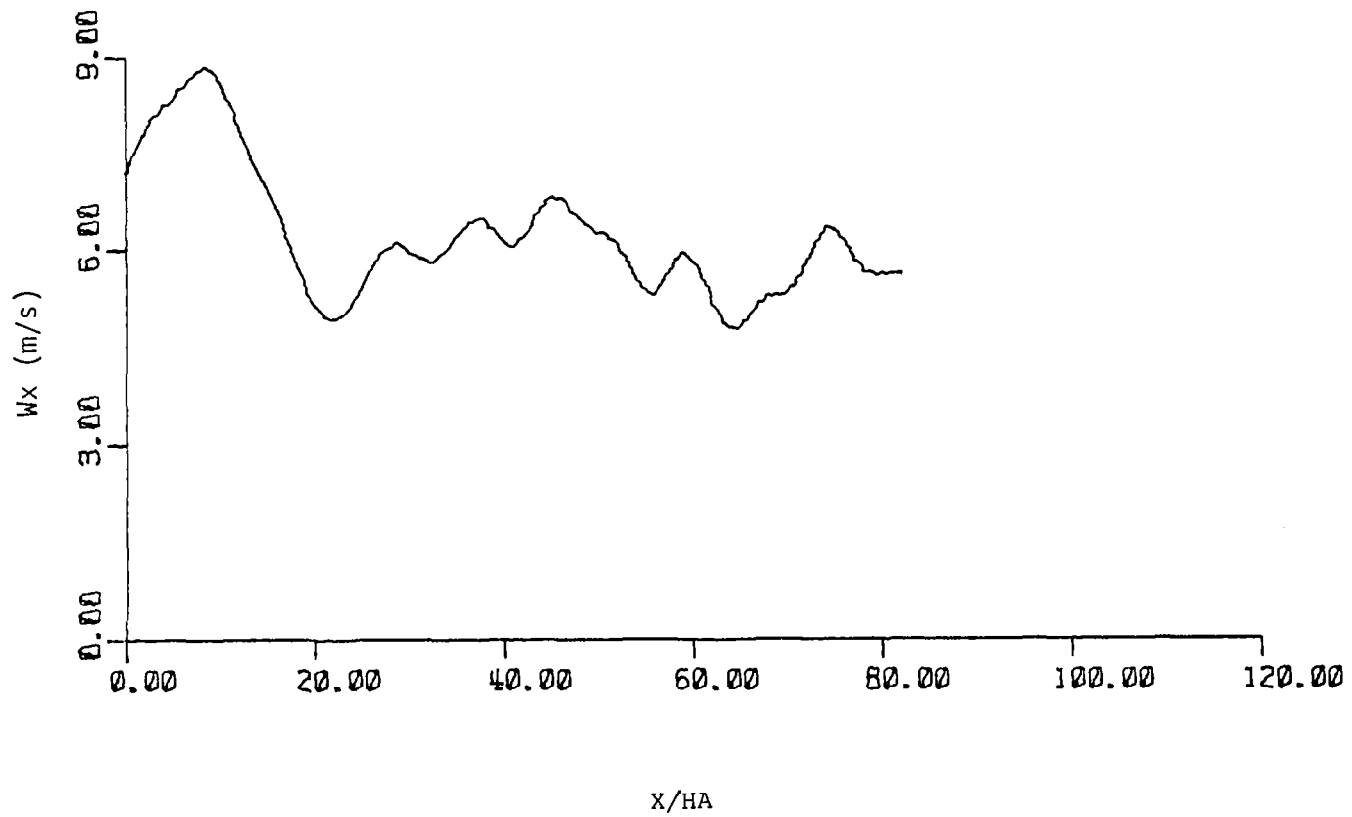
13

Figure 1   Eulerian glide slope wind profile measured by Doppler radar
during Queen Air flight 17/run 2.

horizontal distance traveled. The initial increase and subsequent drop in head wind appears as a wave-form similar to those observed by McCarthy, Blick, and Bensch [3] and Frost and Crosby [4] which cause airspeed and altitude deviations during approach with fixed stick. Figure 2 shows the simulated fixed-stick trajectory of an aircraft having the characteristics of a Queen Air with the phugoidal-type oscillations clearly observable. This is by no means a dangerous approach since the maximum deviation from the glide slope, occurring primarily at the beginning of the approach, is approximately 17 m. The wavelength of the initial wave in the aircraft trajectory measures approximately 2,300 m (peak to peak), with the remaining waves approximately 1,400 m. The phugoid period of the Queen Air (approach speed Va_0 = 56 m/s) as determined by $T = \sqrt{2}\pi Va_0/g$ from Etkin [9] is 25.5 seconds. The Queen Air phugoid wavelength is $\lambda = Va_0 T$ or 1,438 m. However, since this is an approximate value and since a pure sine wave at the Queen Air's phugoid frequency is not specifically input, the exact Queen Air phugoidal wavelength is not expected. The phugoidal-type oscillations are augmented primarily by the initial increase in head wind from 7.21 m/s to 8.84 m/s and subsequent decrease to 4.91 m/s. The increasing head wind causes the initial rise above the glide slope and an initial increase and then decrease of airspeed. Shortly after the airspeed begins to decrease, the head wind begins to decrease and the airplane descends through the glide slope. The initial encounter with this wave sets off the subsequent oscillations where the aircraft descends and picks up airspeed, then begins to ascend until it once again loses airspeed and begins to descend again.

Figure 3 shows the trajectory of a simulated Queen Air under autopilot control descending through the same wind field (Queen Air 17/2). Predictably, the trajectory is perfectly aligned with the glide slope and all phugoidal-type oscillations are removed. Figures 4 and 5 show the minor elevator and thrust control inputs necessary to maintain the approach along the glide slope. The sign conventions for elevator angle are shown in Figure 6. Since the autopilot represents a flight path optimization control system, the initial increasing head wind is countered with slightly increased thrust to maintain ground speed and an

15
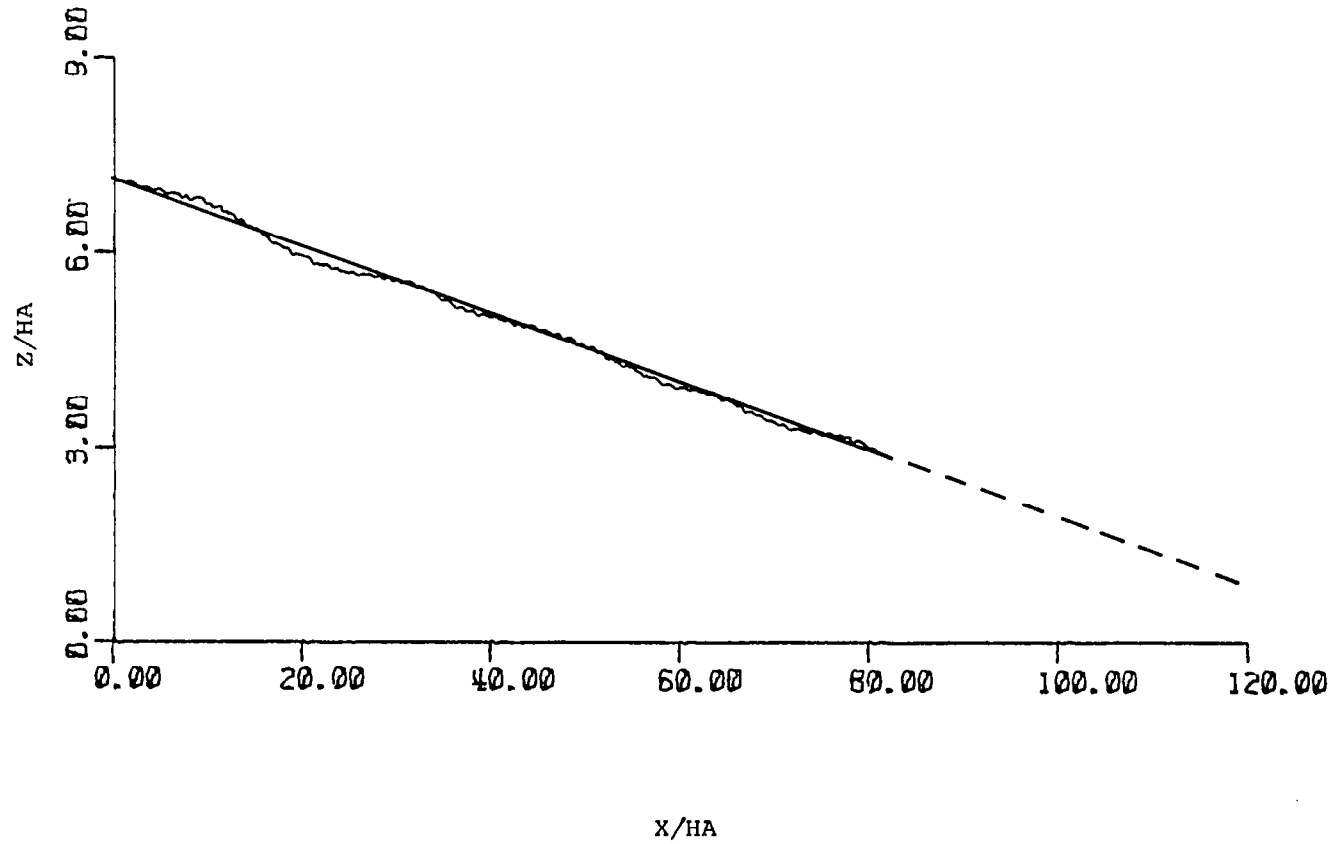
Figure 2   Simulated fixed-stick trajectory of a Queen Air flown through
Queen Air flight 17/run 2 wind profile.

Figure 3 Simulated trajectory of a Queen Air under autopilot control
flown through Queen Air flight 17/run 2 wind profile.

Figure 4 Autopilot elevator inputs to Queen Air in flight through
Queen Air flight 17/run 2 wind profile.

Figure 5 Autopilot thrust inputs to Queen Air in flight through Queen
Air flight 17/run 2 wind profile.
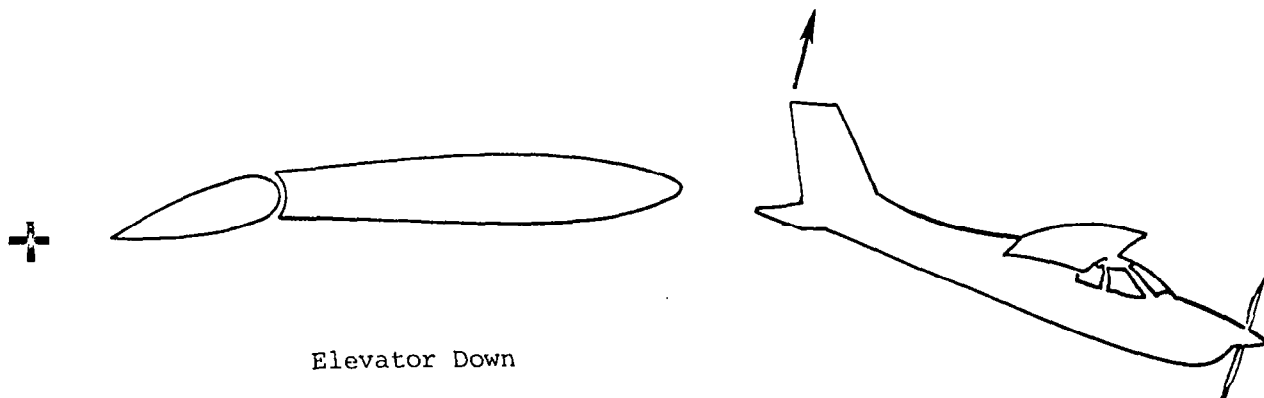
Elevator Down
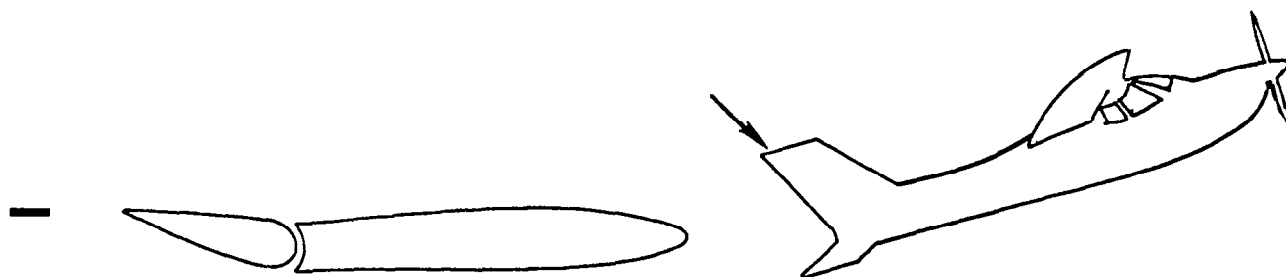
Elevator Up

Figure 6 Elevator angle sign conventions.

elevator setting moving from negative to positive to pitch the nose down to counter the increased rise above the glide slope. As the head wind begins its drop from 8.84 m/s to 4.91 m/s, the initially added thrust is removed to maintain ground speed and the nose is pitched up to arrest descent. The airspeed is still high due to the previously added airspeed due to the thrust increase during the increased head wind.

Throughout the flight, the autopilot tries to closely monitor the aircraft's state (airspeed, ground speed, descent rate, and glide slope alignment) and retrim the aircraft following the changes in the wind.

Figures 7, 8, and 9 show trajectory, elevator angle, and thrust setting for a simulated Queen Air flown by a pilot with a 70 percent performance rating. The control inputs are small and similar to those of the autopilot. This is reasonable since the wind shear in this case is neither large nor severe. Again the aircraft is flown straight down the glide slope with no discernible deviations. Next, a pilot having a lower performance rating of 8 percent is examined. Figures 10, 11, and 12 show the aircraft trajectory and the elevator and thrust control settings. The pilot attempts to retrim to the changing wind trend, but due to slower response time, the control excursions are larger than those of the autopilot and the 70 percent rated pilot. The trajectory shows that the pilot cannot adequately counter the initial head wind increase, and a small rise above the glide slope can be seen. However, the pilot manages to get back to the glide slope, suggesting that the main concern in maintaining control is the initially encountered wave and that controlling the remainder of the run is relatively straight-forward. Finally, a simulated Queen Air commanded by a pilot having a 5.5 percent performance rating was flown through the wind field. The performance rating in this case appears to be the threshold of minimum control because, as shown in Figure 13, the pilot is unable to counter the effects of the initial wave. The aircraft oscillates about the glide slope until finally near the end of the run the pilot is able to bring the plane back to intercept the glide slope. The elevator and thrust control inputs are presented in Figures 14 and 15, respectively.

Figure 7   Simulated trajectory of a Queen Air controlled by a 70 percent
performance rated pilot flown through Queen Air flight 17/run 2
wind profile.

Figure 8 Elevator inputs by 70 percent rated pilot to Queen Air flown
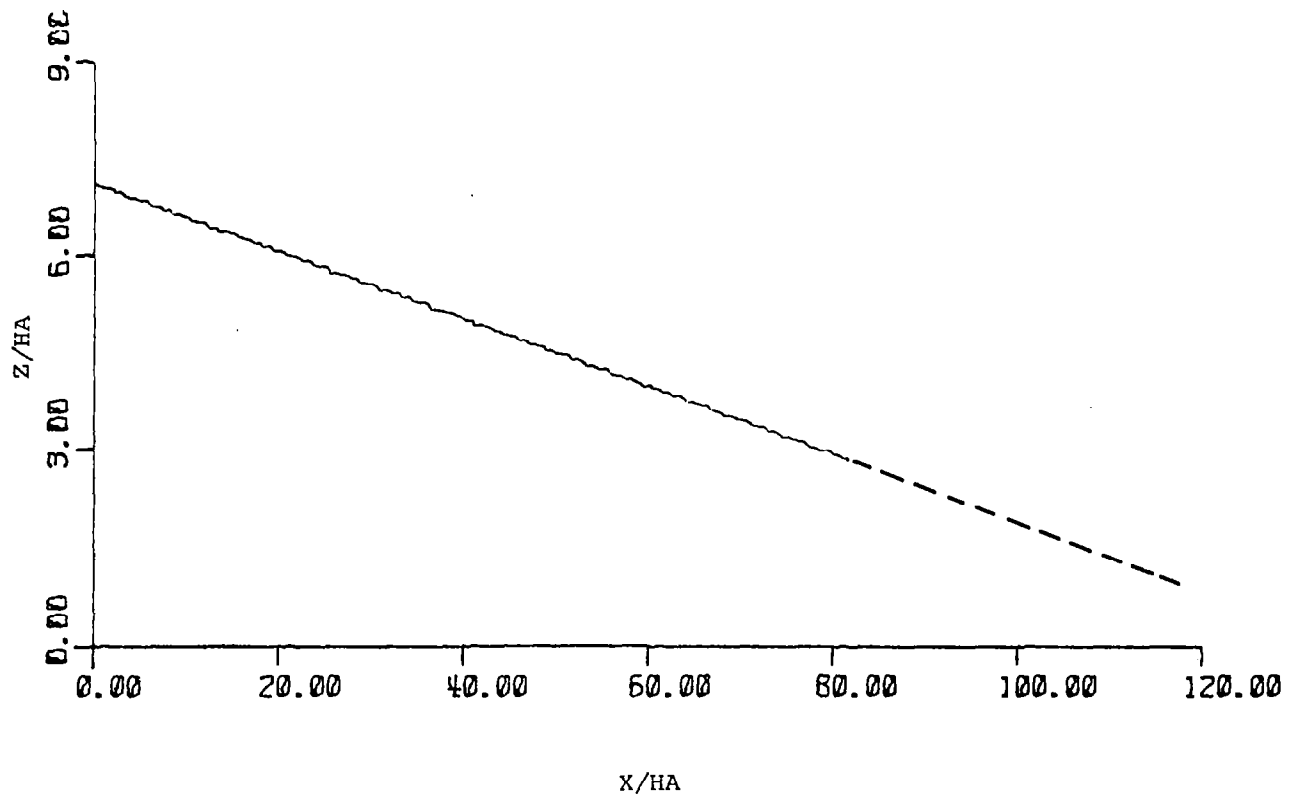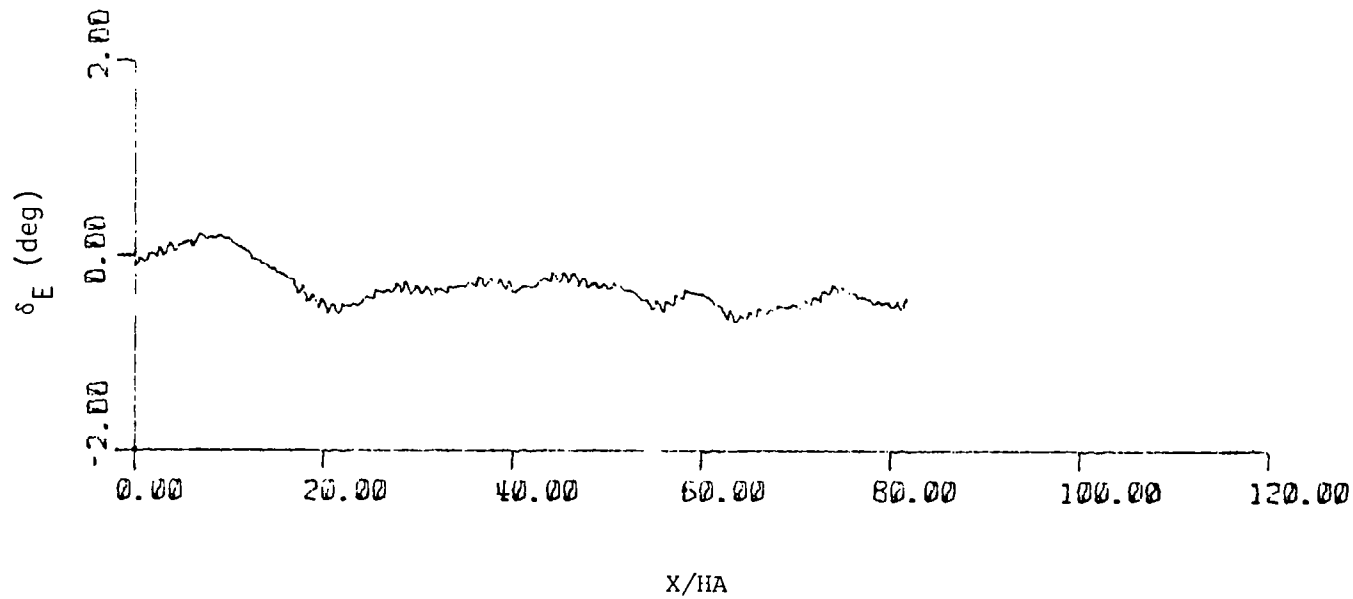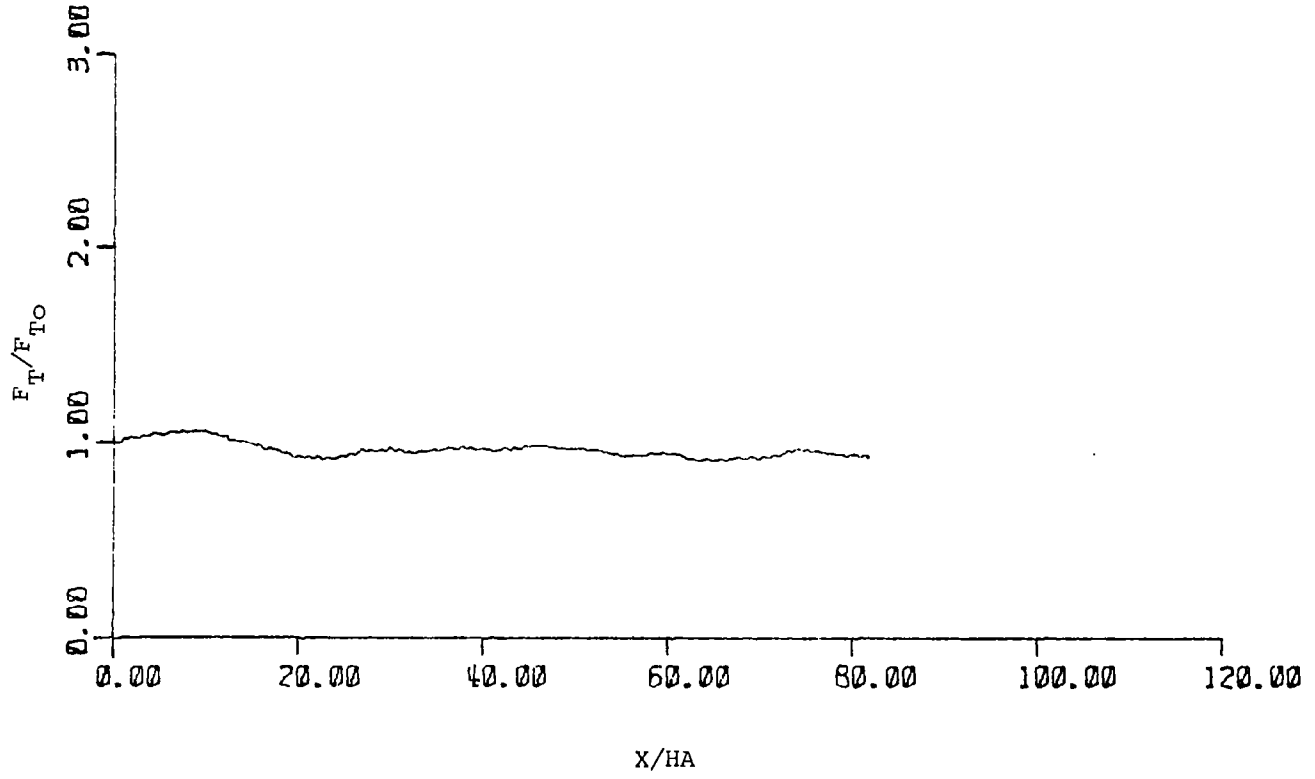through Queen Air flight 17/run 2 wind profile.

Figure 9 Thrust inputs by 70 percent rated pilot to Queen Air flown through
Queen Air flight 17/run 2 wind profile.

Figure 10   Simulated trajectory of a Queen Air controlled by an 8 percent
performance rated pilot flown through Queen Air flight 17/run 2
wind profile.

Figure 11   Elevator inputs by 8 percent rated pilot to Queen Air flown
through Queen Air flight 17/run 2 wind profile.

Figure 12   Thrust inputs by 8 percent rated pilot to Queen Air flown through
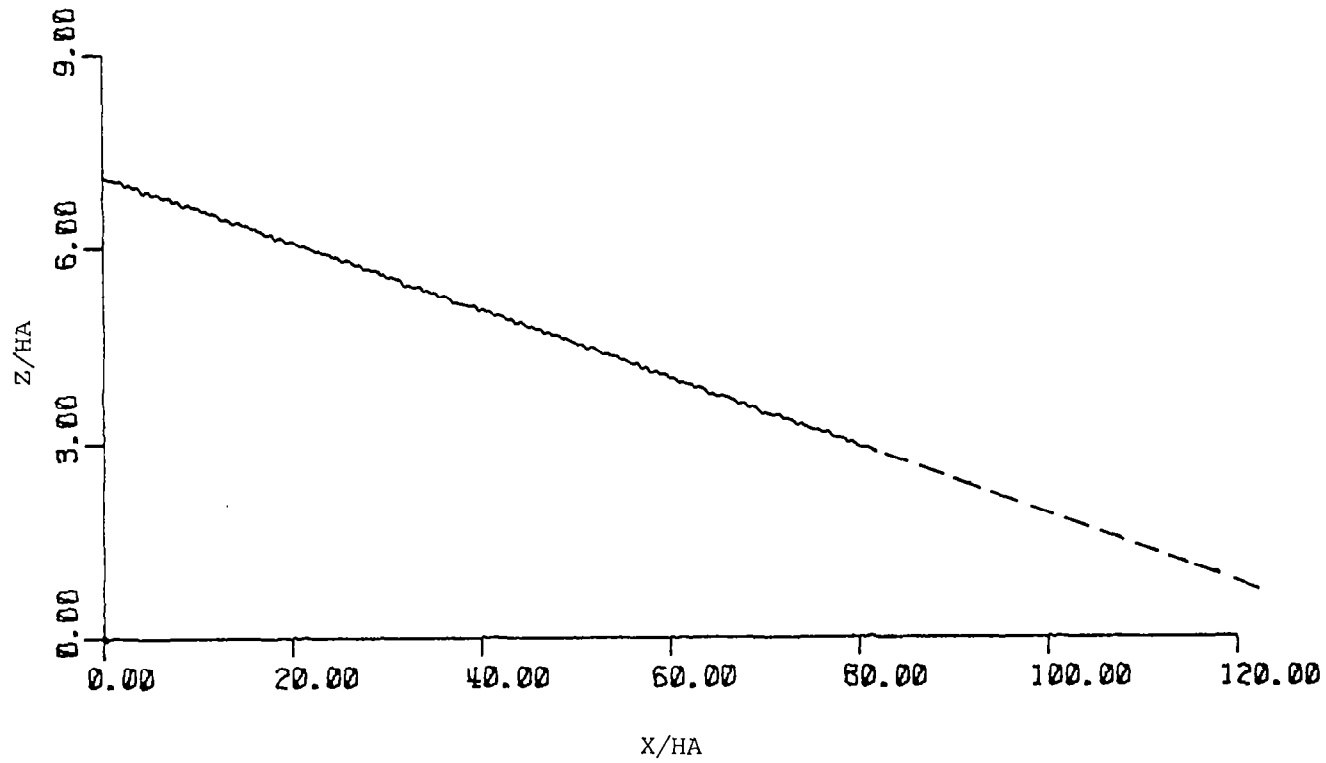Queen Air flight 17/run 2 wind profile.

Figure 13   Simulated trajectory of a Queen Air controlled by a 5.5 percent
performance rated pilot flown through Queen Air flight 17/run 2
wind profile.
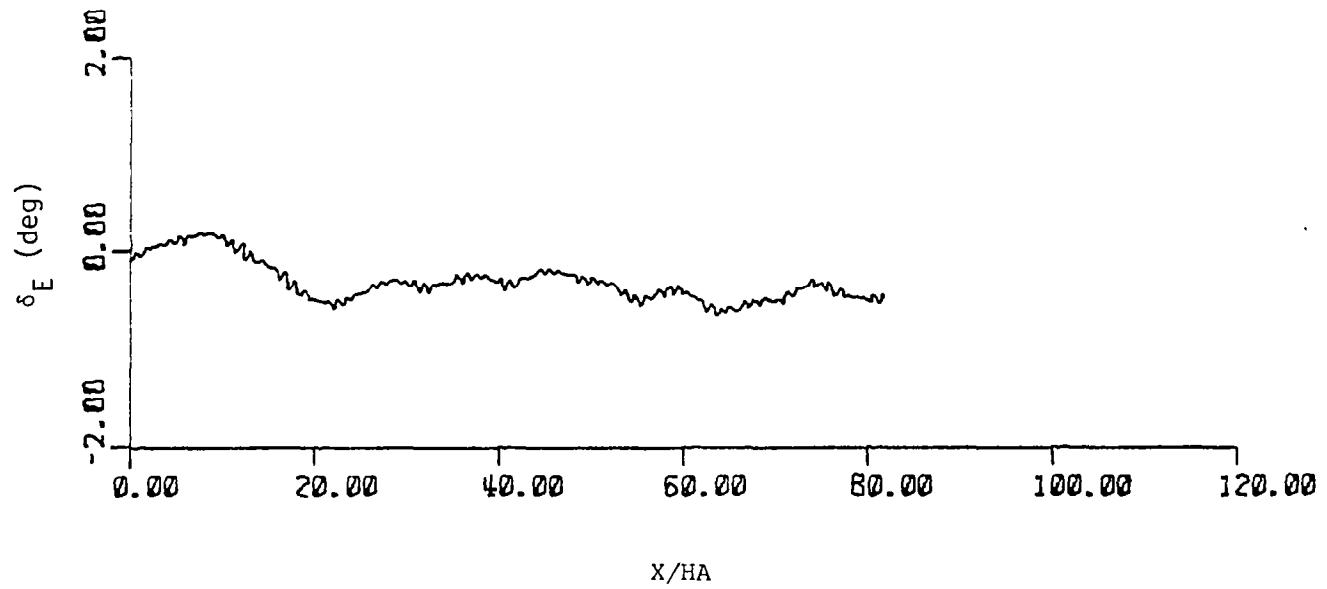
Figure 14   Elevator Inputs by 5.5 percent rated pilot to Queen Air flown
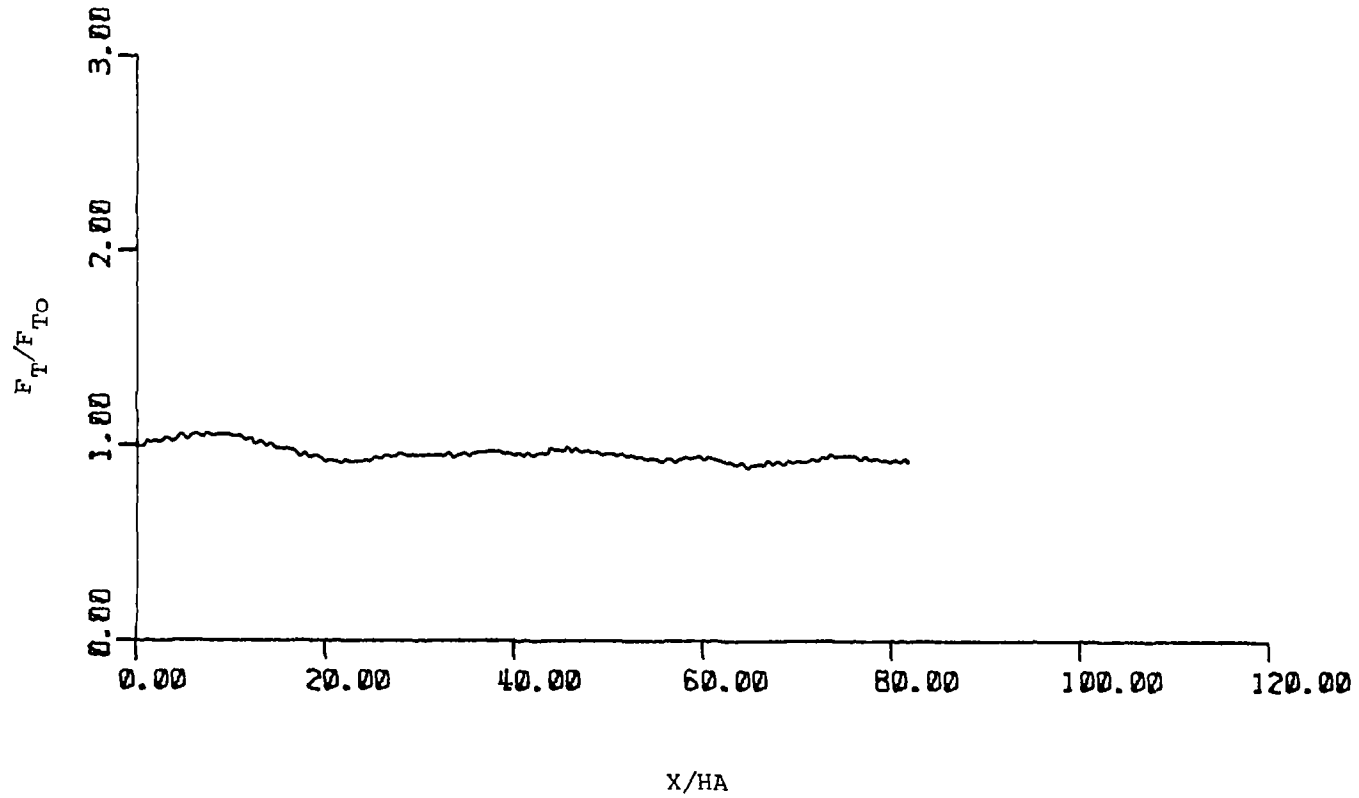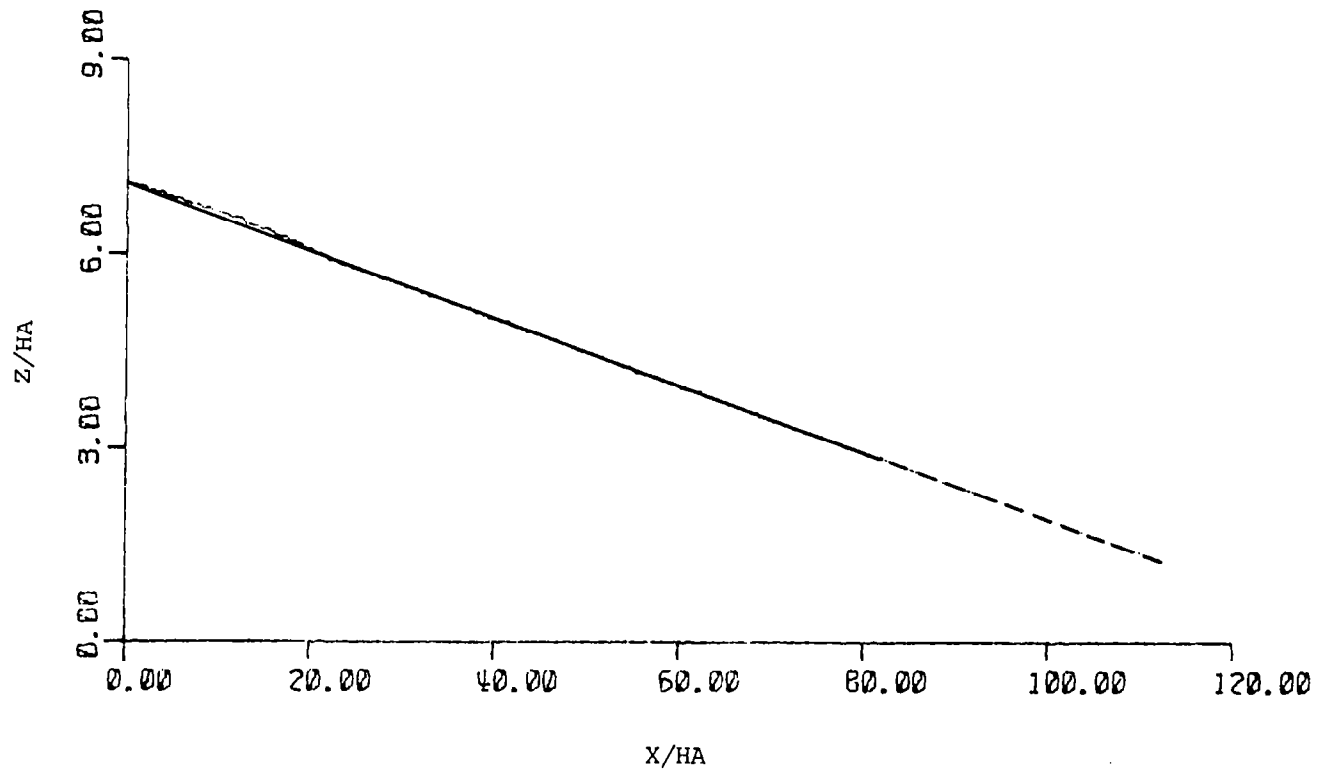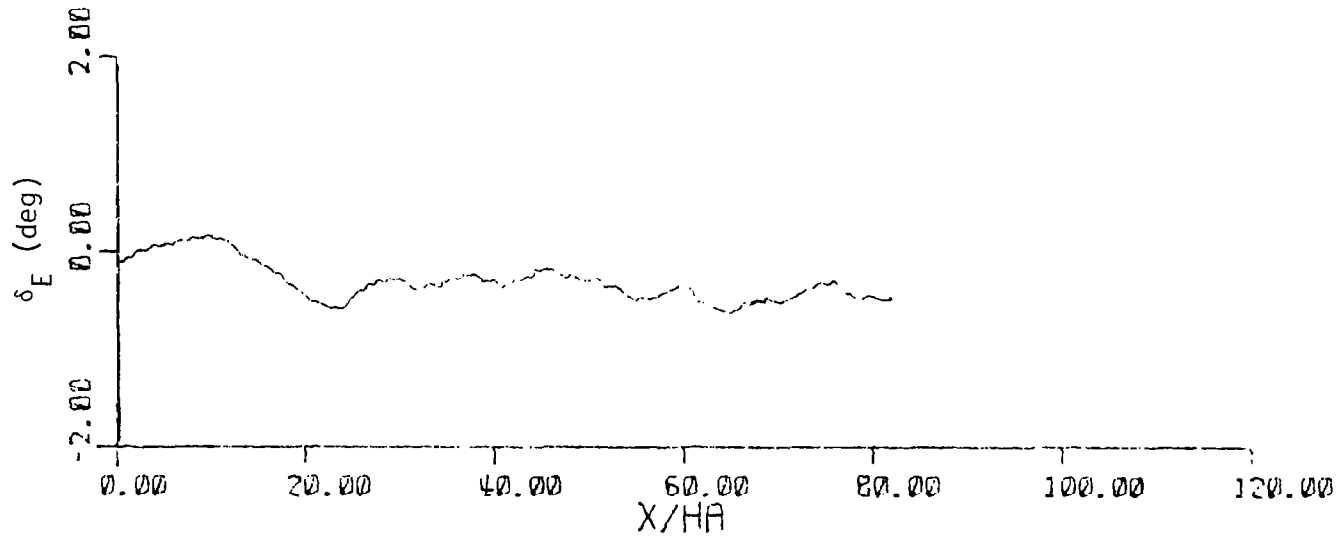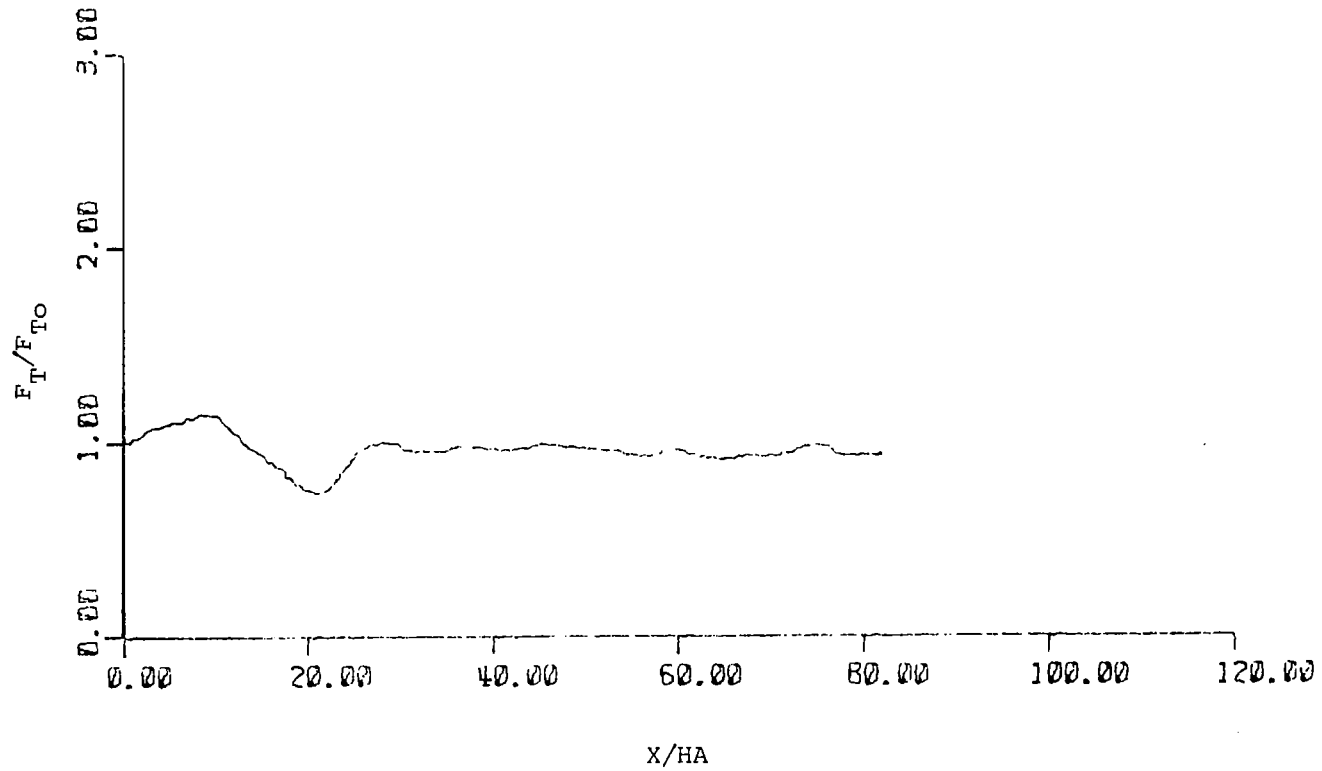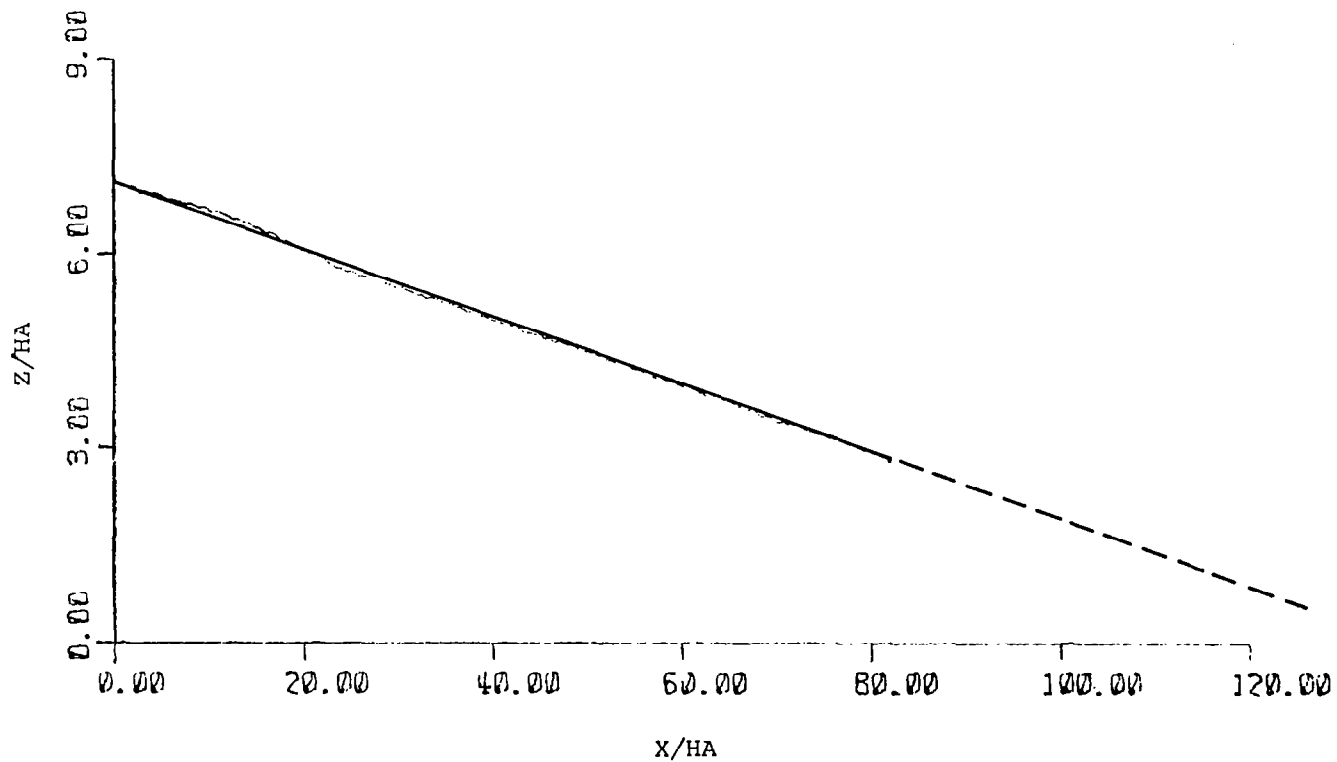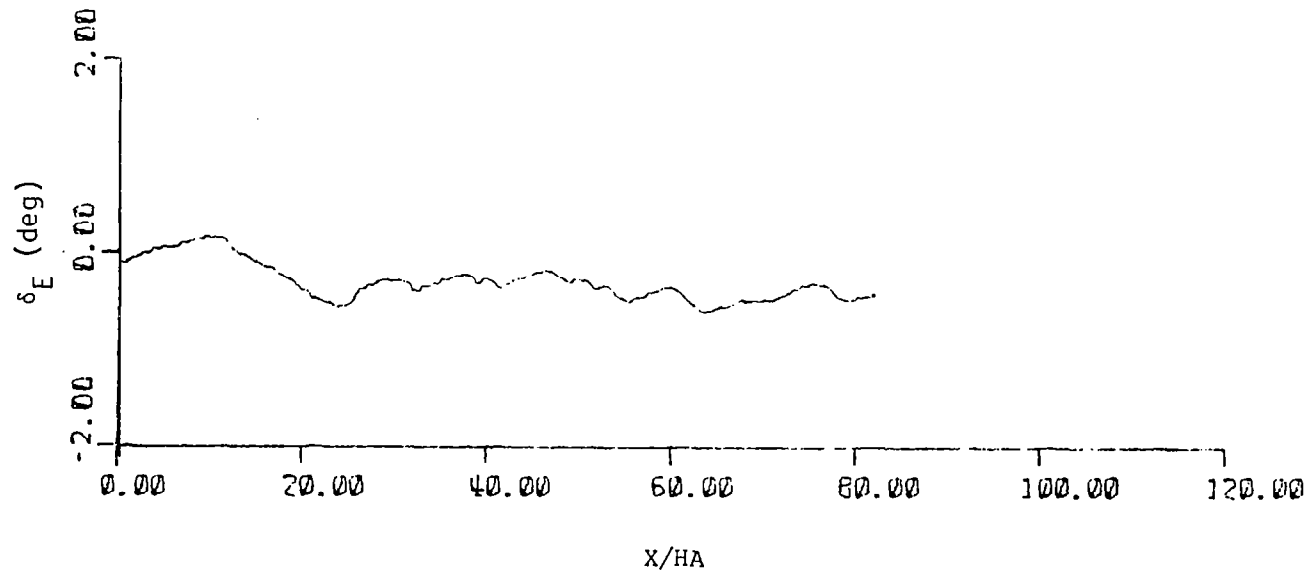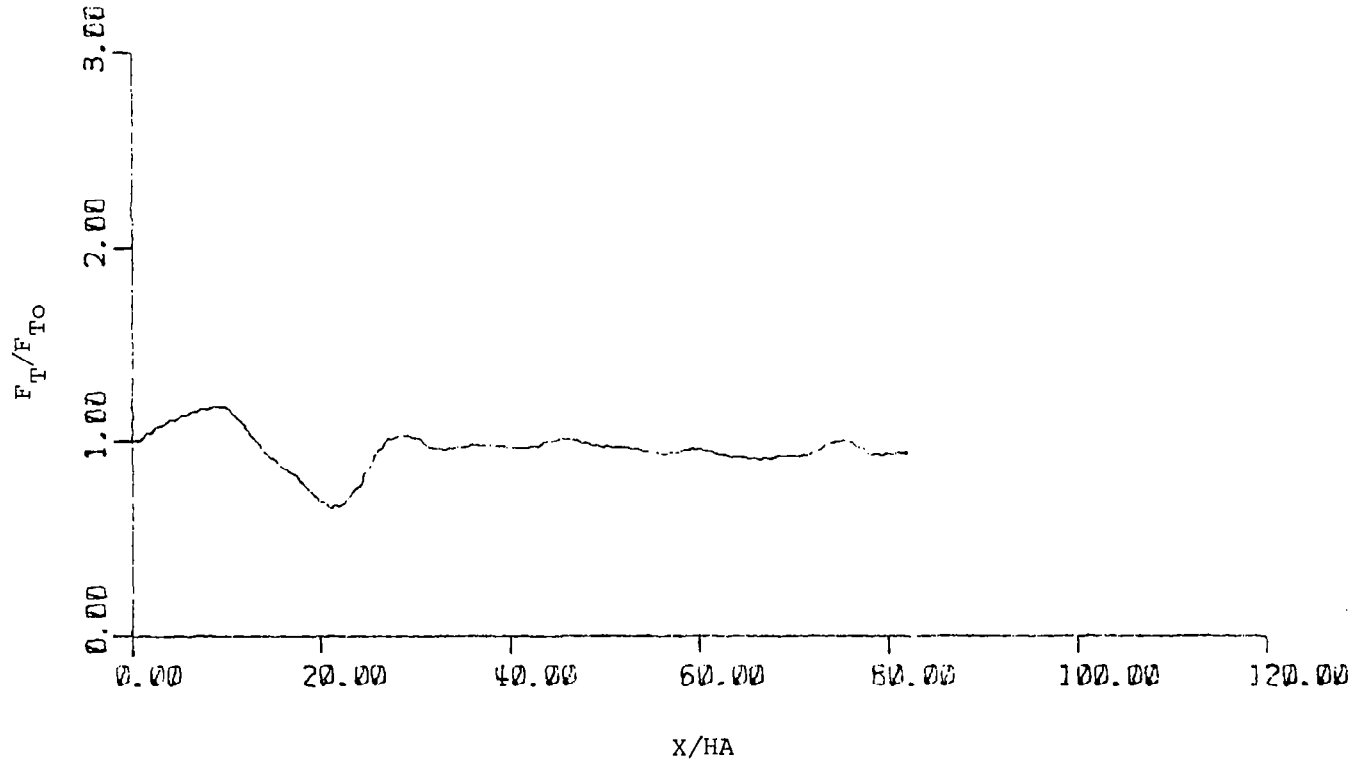through Queen Air flight 17/run 2 wind profile.

Figure 15   Thrust inputs by 5.5 percent rated pilot to Queen Air flown
through Queen Air flight 17/run 2 wind profile.

The results of this simulation show that, although the aircraft is disturbed by the wind field in the fixed-stick case, the shear does not appear to be strong enough to cause any difficulty to a human-controlled vehicle. This is verified by the extremely low performance rated pilots who are able to make excellent approaches.

5.2 Simulated Boeing 727 Flight Through Queen Air Flight 17/Run 2 Wind Field

An aircraft having the characteristics of a Boeing 727 is flown in simulated flight through the same wind field that the Queen Air encountered. The time history wind data, which have been converted from range data using the Queen Air's average airspeed, were reconverted to range data so that both aircraft encounter essentially the same wind field. The approach speed used for the B727 runs is 72 m/s as opposed to 56 m/s for the Queen Air.

Figure 16 shows the fixed-stick flight of the simulated B727 through the Queen Air wind field. As with the Queen Air, the B727 encounter with the initial increasing and decreasing head wind results in a phugoidal-type oscillation in the trajectory. These oscillations are of higher amplitude and lower damping than those of the Queen Air. This is in direct agreement with McCarthy, Blick, and Bensch [3] and Frost and Crosby [4], who suggest that large commercial transports will experience greater difficulty in flight through wind shear than smaller aircraft due to the effects of higher landing speed and higher lift-to-drag ratio influence on the exponential phugoid damping period. Table 2 shows comparative calculations for the B727 and Queen Air exponential phugoid damping periods. The greatest deviation from the glide slope in Figure 16 is approximately 43 m. The phugoid time period for the B727 given by $T = \sqrt{2}\pi V_{a_0}/g$ is 32.5 sec and the wavelength $\lambda = V_{a_0}T$ is 2,341 m as compared with the 2,743 m (peak to peak) waves of the simulated trajectory.

The trajectory of a simulated B727 flown by autopilot through the wind field is shown in Figure 17. Predictably the flight is smooth and perfectly aligned with the glide slope. In Figure 18 it can be observed that the response of the autopilot to the initial head wind increase is

31
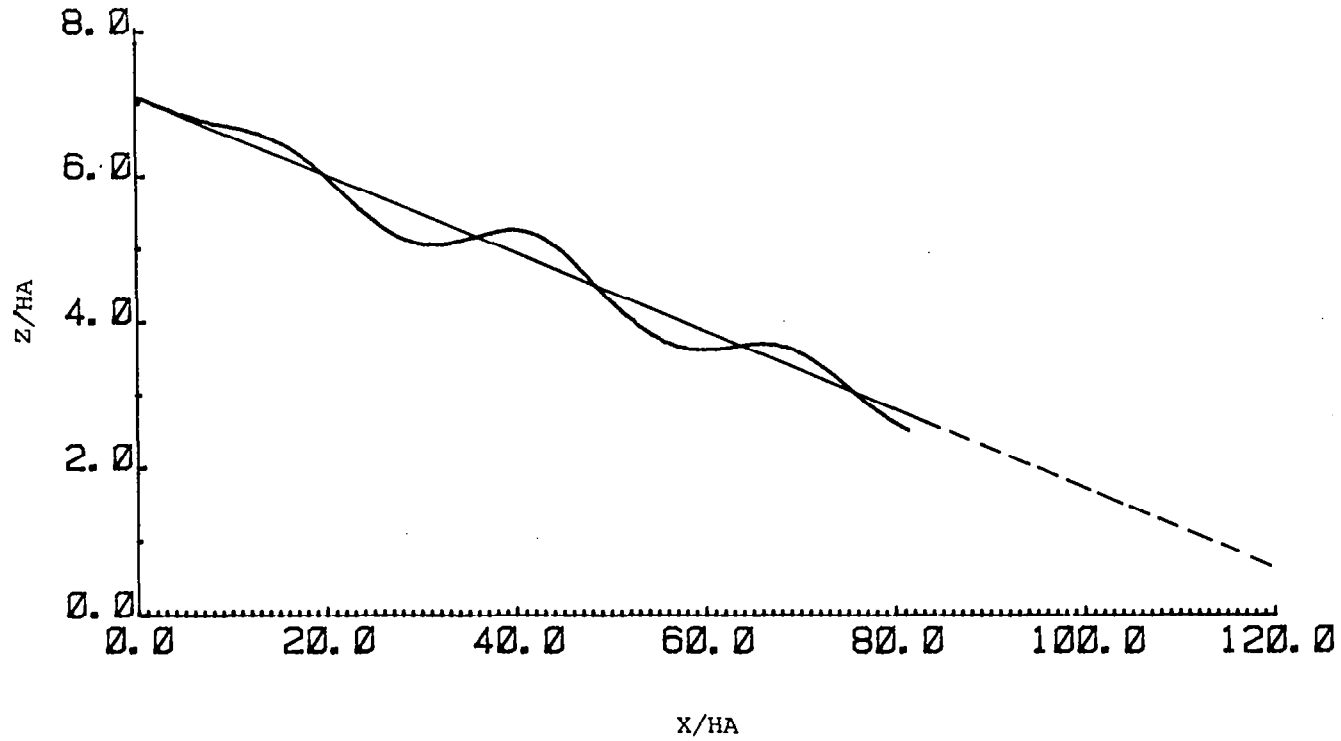
Figure 16 Simulated fixed-stick trajectory of a B727 flown through Queen
Air flight 17/run 2 wind profile.

TABLE 2. Comparison of Exponential Phugoid Damping Periods (T) of Queen
Air and Boeing 727.

T = the time for the phugoid oscillation to decay to 1/e of its initial
amplitude.

$$T = \frac{V_{a_0}}{g} \frac{C_{L_0}}{C_{D_0}}$$

where

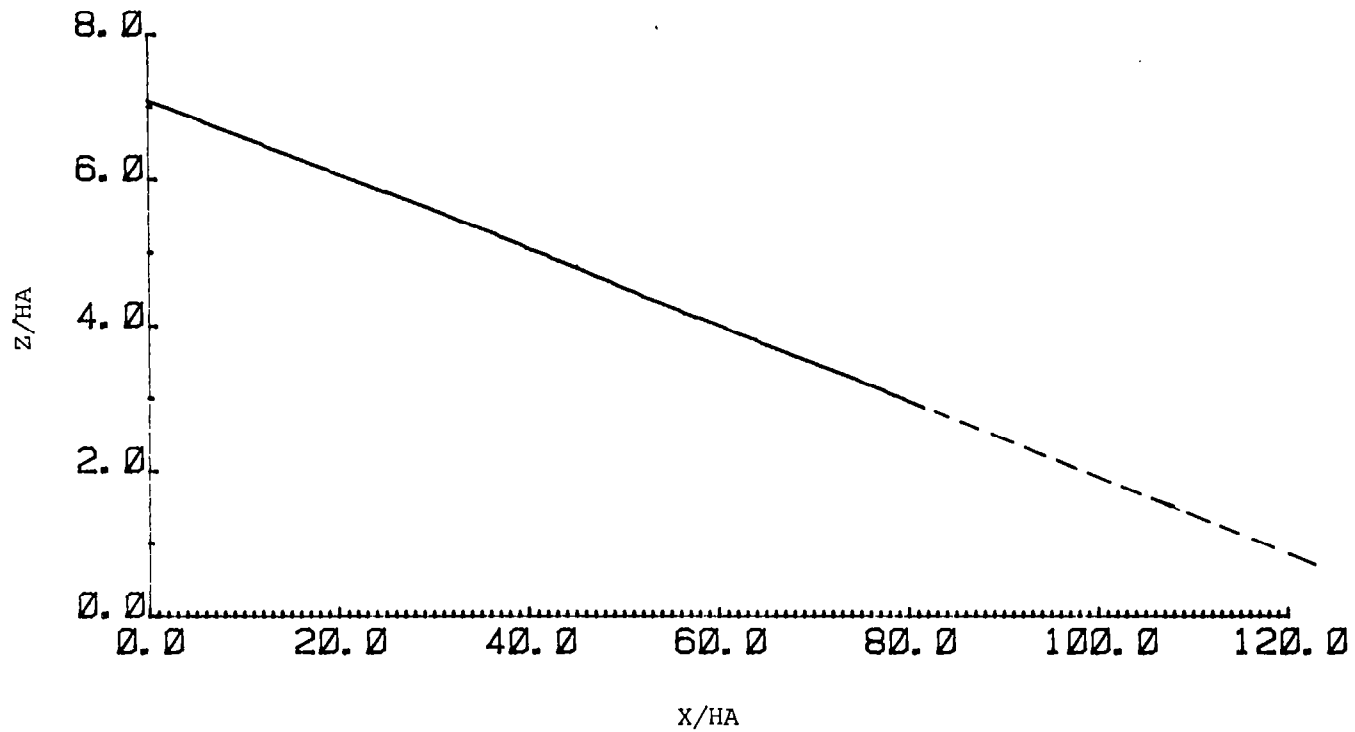|	Boeing 727	Queen Air
V_{a_0} = approach airspeed (m/s)	72.000	56.000
g = gravitational acceleration (m/s^2)	9.800	9.800
C_{L_0} = lift coefficient (dimensionless)	1.360	0.639
C_{D_0} = drag coefficient (dimensionless)	0.139	0.080
T = exponential phugoid damping period (sec)	71.700	45.900

Figure 17   Simulated trajectory of a B727 under autopilot control flown
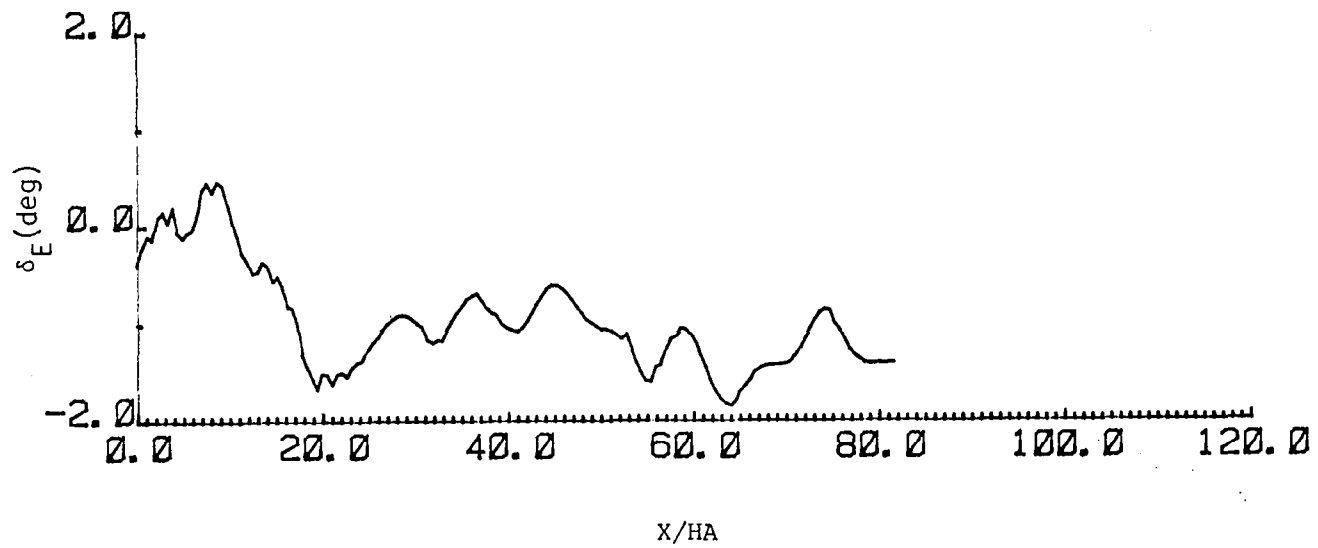through Queen Air flight 17/run 2 wind profile.

Figure 18 Autopilot elevator inputs to B727 in flight through Queen Air
flight 17/run 2 wind profile.

a positive deflection in elevator angle. This pitches the nose down to counter the nose-up attitude caused by the increased head wind. However, in Figure 19 it is noticed that the autopilot optimization control loop has decreased thrust when encountering the increased head wind at the beginning of the run. With the Queen Air, thrust was increased to maintain ground speed. In the case of the B727, the higher approach airspeed into the increasing head wind causes too much additional lift which tends to force the airplane above the glide slope. Thus, the thrust was cut back to prevent the climb above the glide slope. It should also be noted that the elevator and thrust control inputs to the B727 are of larger magnitude than those of the Queen Air.

The trajectory of an aircraft controlled by a pilot with a 70 percent performance rating is given in Figure 20. The aircraft flies straight down the glide slope. Figures 21 and 22 provide the elevator and thrust control inputs which are similar in magnitude to those made by the autopilot.

The flight of an aircraft flown by a pilot with a low performance rating (5.5 percent) is next considered. The flight profile (Figure 23) shows that this pilot is unable to fully counter the initial increased head wind and the aircraft rises slightly above the glide slope at the beginning of the run. Following a slight descent below the glide slope due to the decreasing head wind, the pilot manages to correct and maintain a near-perfect approach. Note that the elevator and thrust controls (Figures 24 and 25) show less "fine tuning" than those of the 70 percent rated pilot.

This above-described simulation shows that although the aircraft oscillates due to the wind shear for the fixed-stick run, there is no problem in maintaining an excellent approach in a piloted aircraft even for a pilot with a low performance rating (5.5 percent).

5.3 Simulated B727 Flight Through Sinusoidal 6 m/s Amplitude Wave Near Phugoid Frequency

A simulation is carried out flying the simulated B727 through a 6 m/s head wind shearing to a 6 m/s tail wind. This wave disturbance is
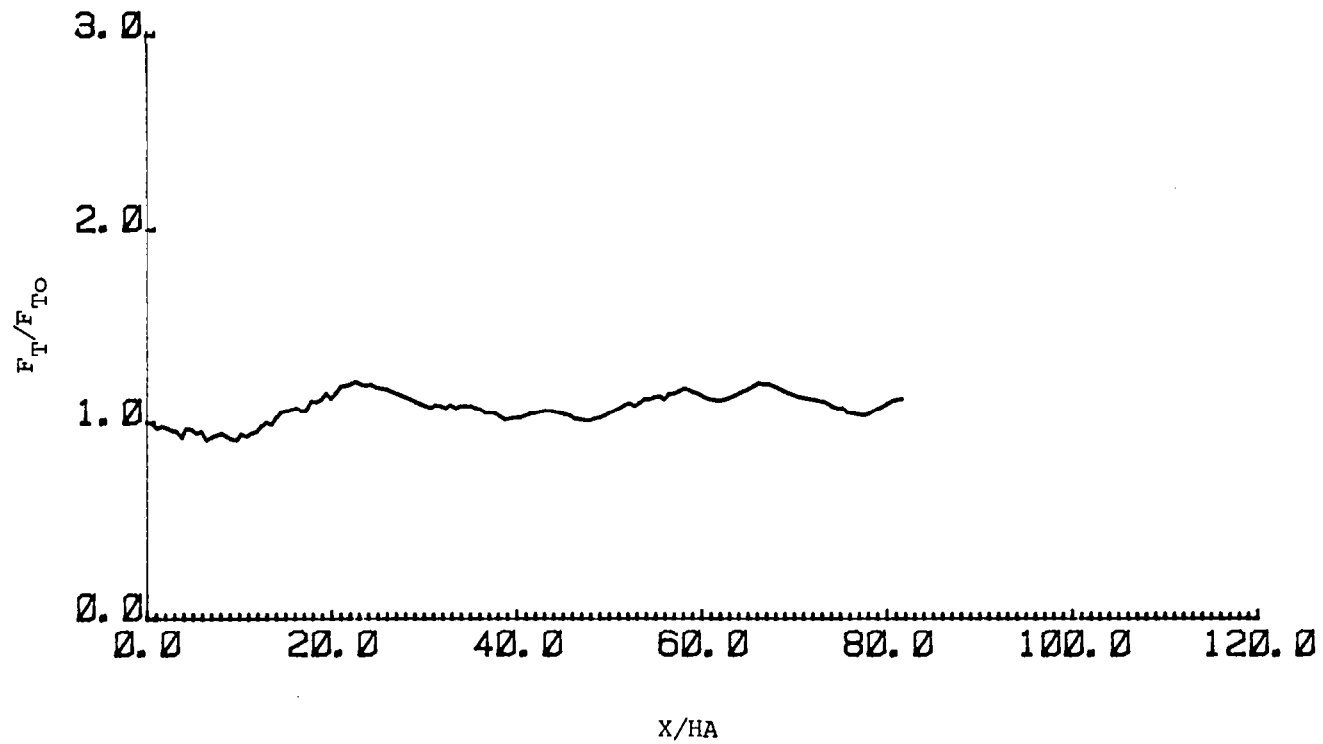
Figure 19   Autopilot thrust inputs to B727 in flight through Queen Air
flight 17/run 2 wind profile.
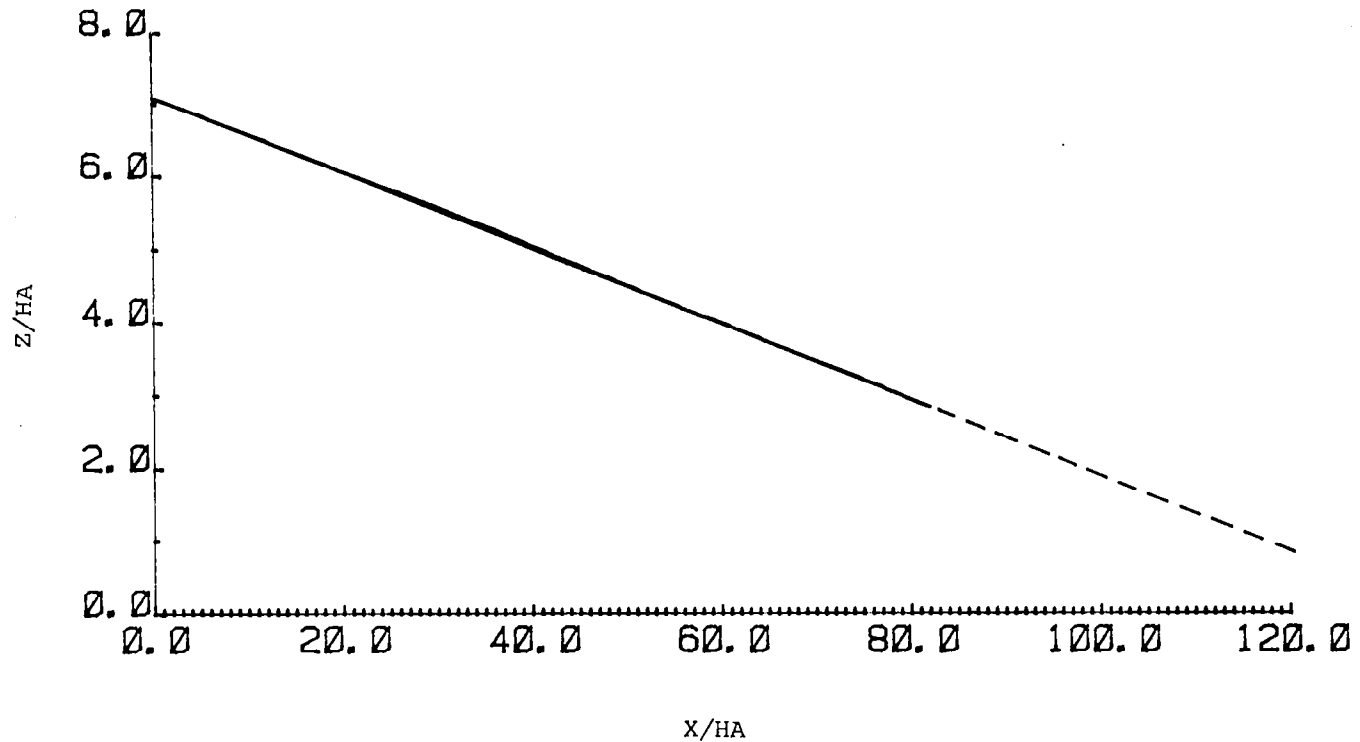
Figure 20   Simulated trajectory of a B727 controlled by a 70 percent
performance rated pilot flown through Queen Air flight 17/
run 2 wind profile.
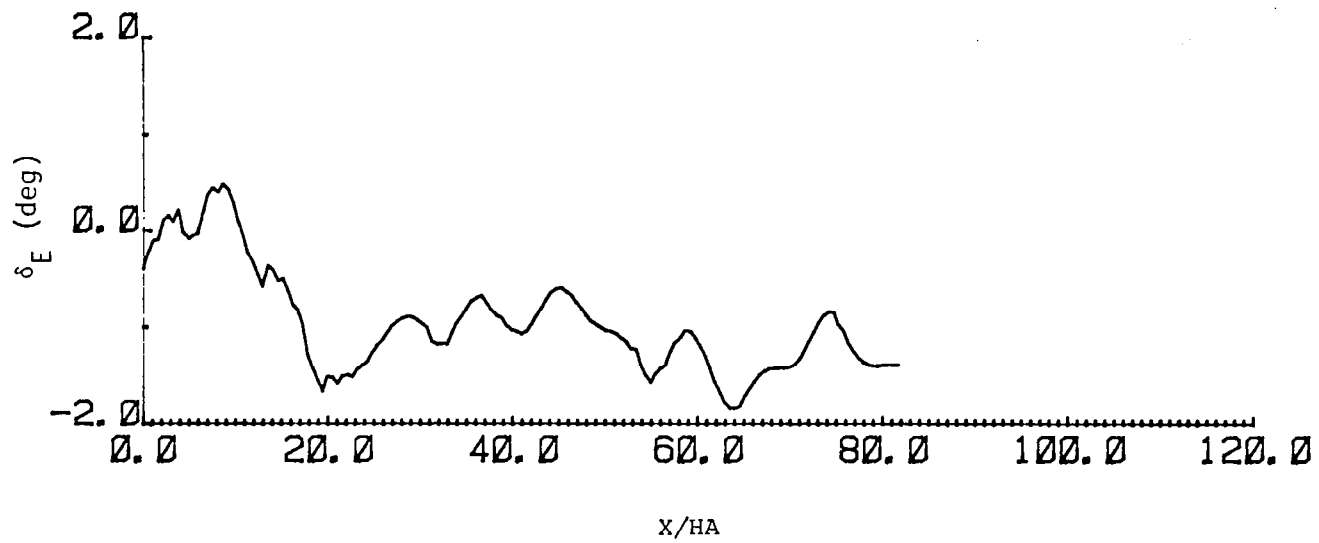
Figure 21   Elevator inputs by 70 percent rated pilot to B727 flown through
Queen Air flight 17/run 2 wind profile.
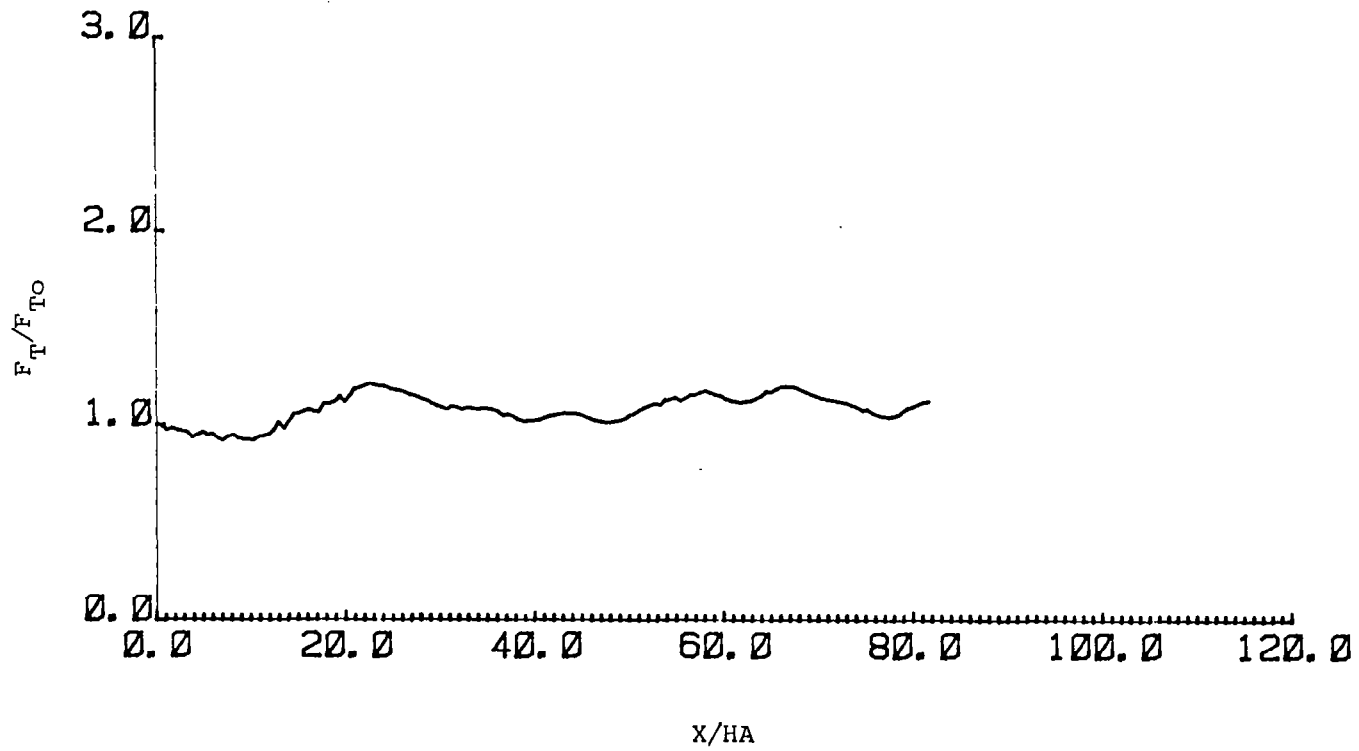
Figure 22   Thrust inputs by 70 percent rated pilot to B727 flown through Queen Air flight 17/run 2 wind profile.
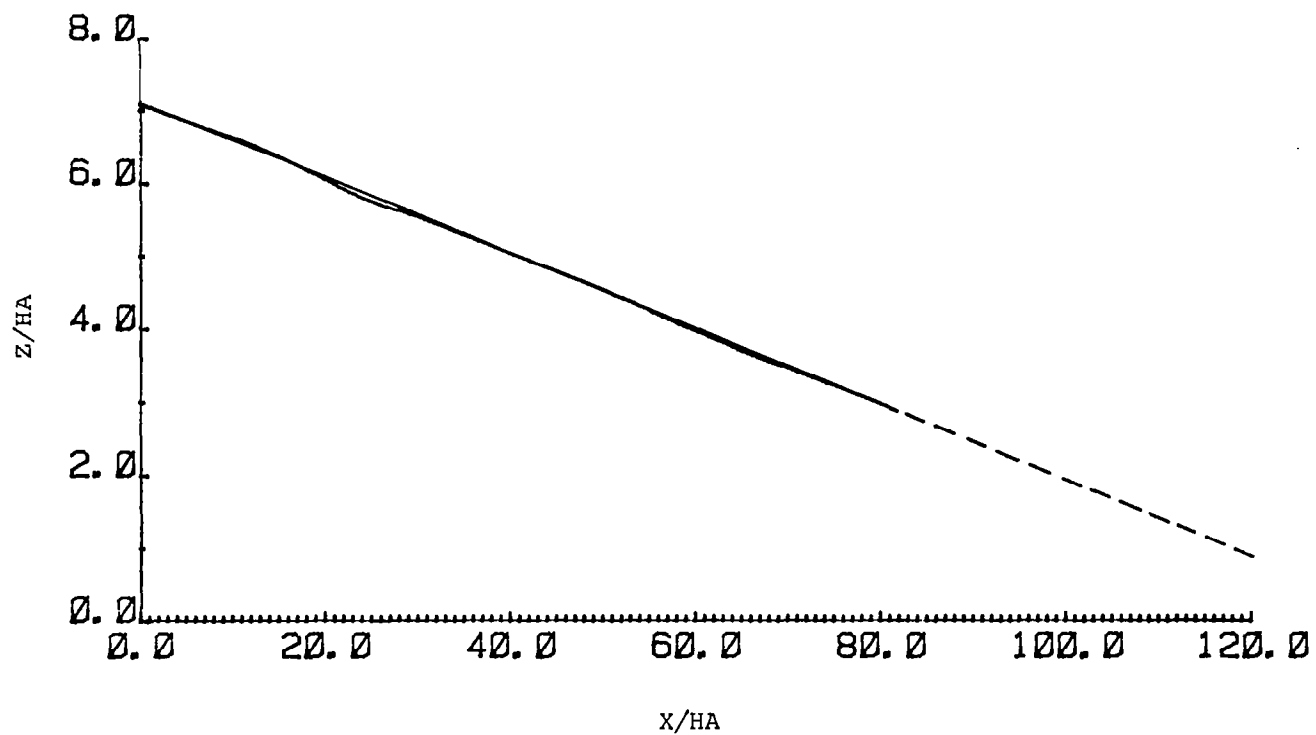
Figure 23   Simulated trajectory of a B727 controlled by a 5.5 percent
           performance rated pilot flown through Queen Air flight 17/run 2
           wind profile.
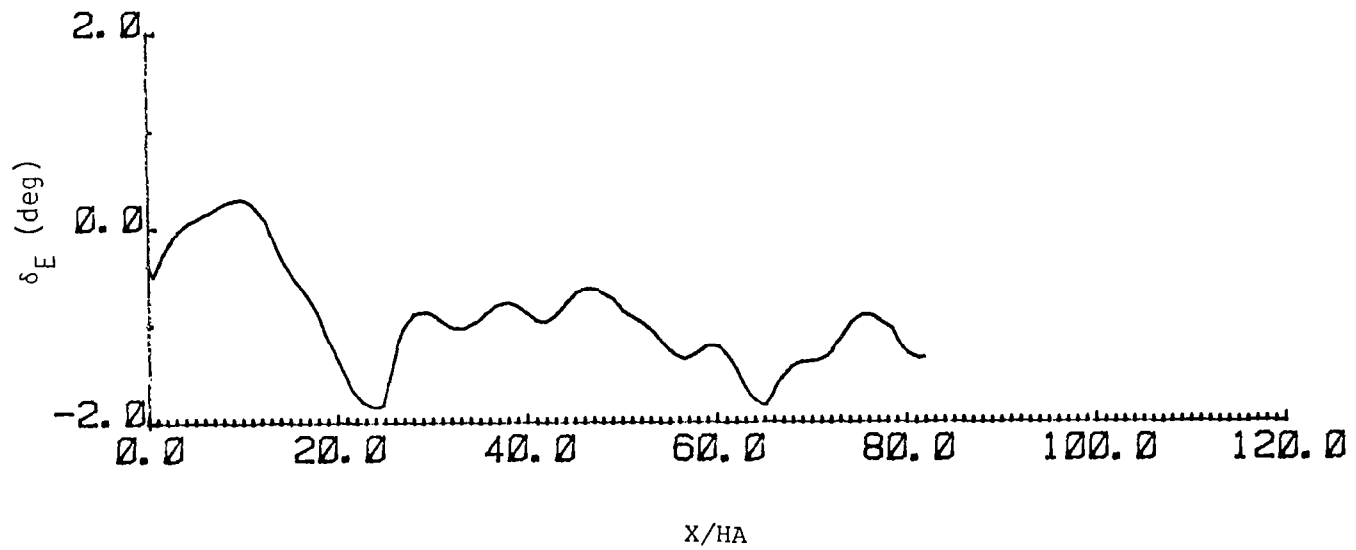
Figure 24   Elevator inputs by 5.5 percent rated pilot to B727 flown through
Queen Air flight 17/run 2 wind profile.
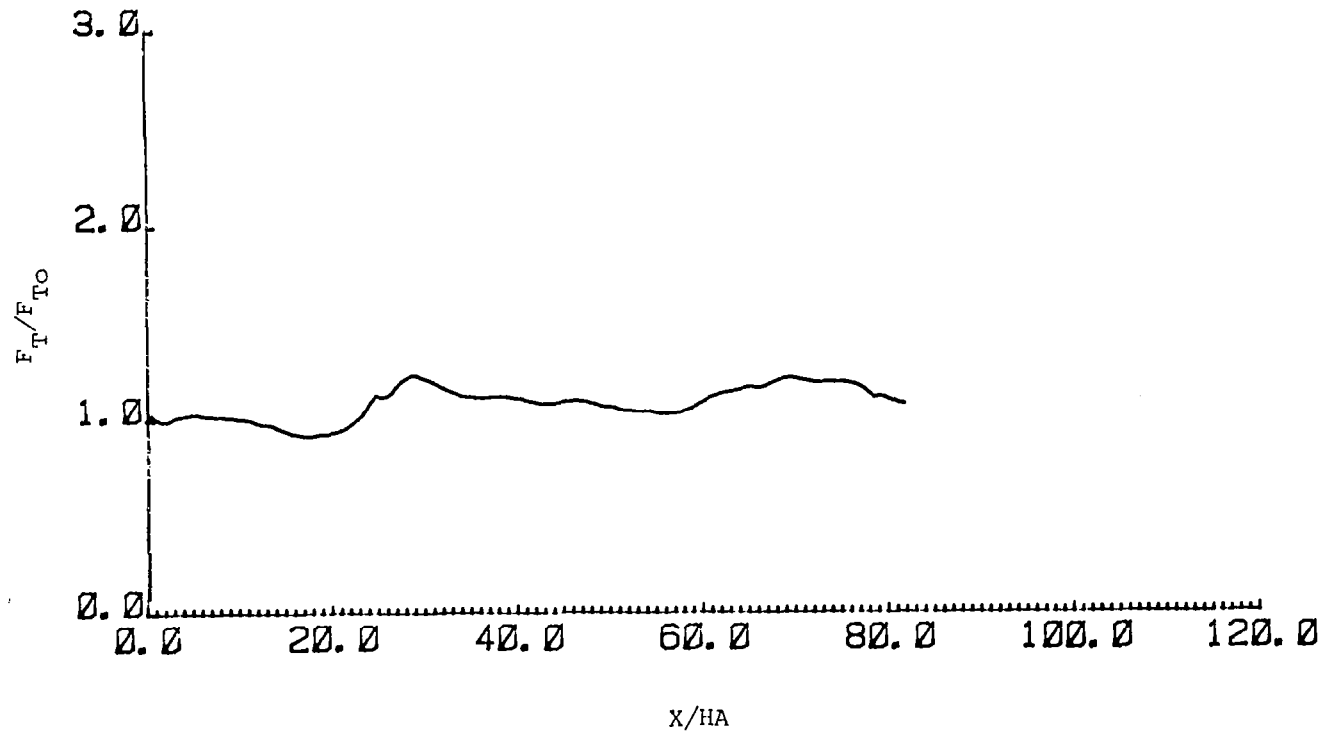
Figure 25   Thrust inputs by 5.5 percent rated pilot to B727 flown through
Queen Air flight 17/run 2 wind profile.

similar to that of the Queen Air 17/2 case except that a wave at approximately the B727's phugoid frequency is encountered by the aircraft. Such a wave disturbance is used to simulate the thunderstorm cell wind environment which has been the cause of either an accident or, at minimum, an incident to several aircraft which encountered similar waves. An aircraft flying through a thunderstorm initially flies into a head wind (the thunderstorm cell outflow). This longitudinal head wind component diminishes to zero as the aircraft flies through the central down draft region of the cell and becomes a tail wind as the aircraft flies into the outflow on the other side.

Figure 26 shows the fixed-stick trajectory of the simulated B727 flying into a constant 6 m/s head wind which begins to decrease at X/HA = 8.3 to become a 6 m/s tail wind at X/HA = 21.2. The aircraft drops below the glide slope and loses airspeed until X/HA = 14.8 when the airspeed starts to increase again. However, since the head wind is still decreasing, the aircraft continues to fall as the airspeed continues to build up. Finally, the aircraft then begins to climb at X/HA = 33. The encountered wave disturbance thus sets off phugoidal oscillations in the trajectory. Since the sinusoidal wind velocities are computed using a time scale based on aircraft position along the glide slope and average approach speed, the sine wave is approximate since the aircraft does not travel collocationally along the glide slope during the wave encounter.

The flight path of a simulated B727 flown by the autopilot is given in Figure 27. The beginning of a very slight descent below the glide slope occurs at X/HA = 11, which is the same location that the fixed-stick aircraft (Figure 26) begins to drop. The autopilot, however, quickly begins to pitch the aircraft nose-up (Figure 28) and increases the thrust (Figure 29) to counter the loss of airspeed and deviation below the desired glide path. The aircraft comes back up to intercept the glide slope and continues the approach through the remaining 6 m/s tail wind without deviation. Note that the retrim for maintaining flight through the tail wind requires a higher thrust setting than for the initial head wind as well as an elevator angle setting of approximately -8°. Once again it can be observed that by correct countering of the wave-form wind

44
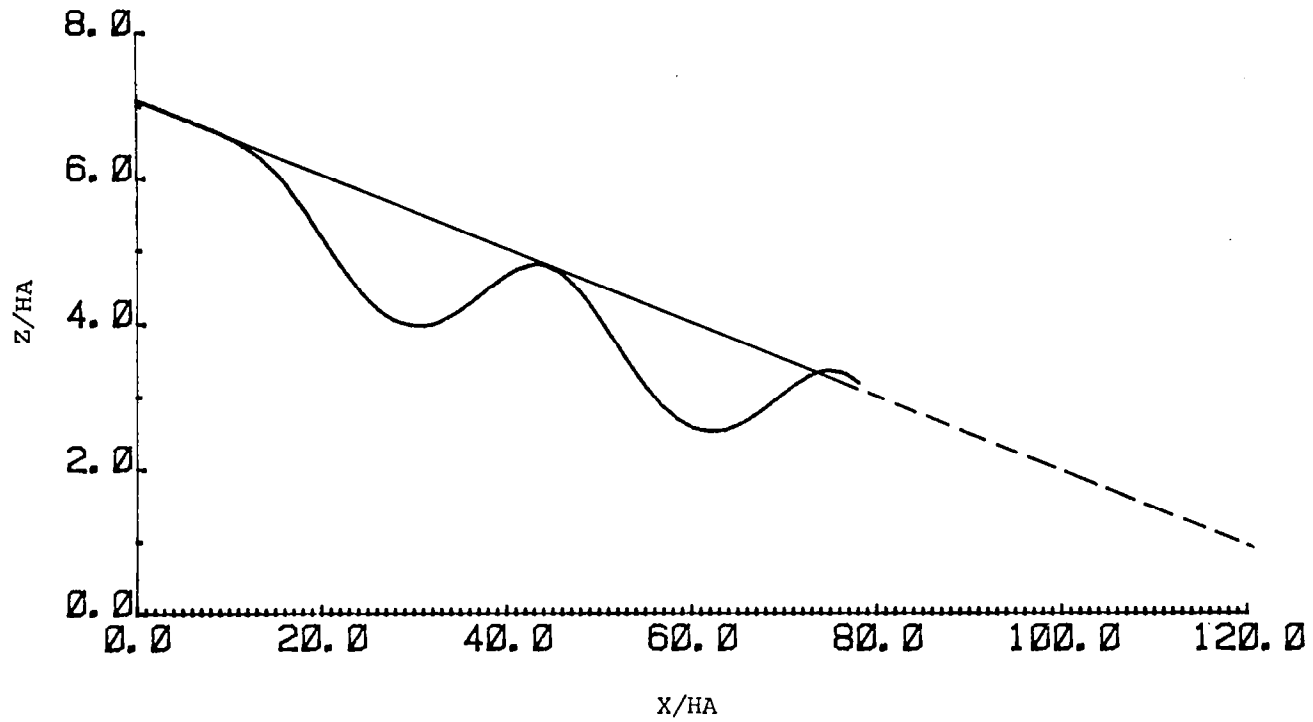
Figure 26   Simulated fixed-stick trajectory of a B727 flown through a 6 m/s
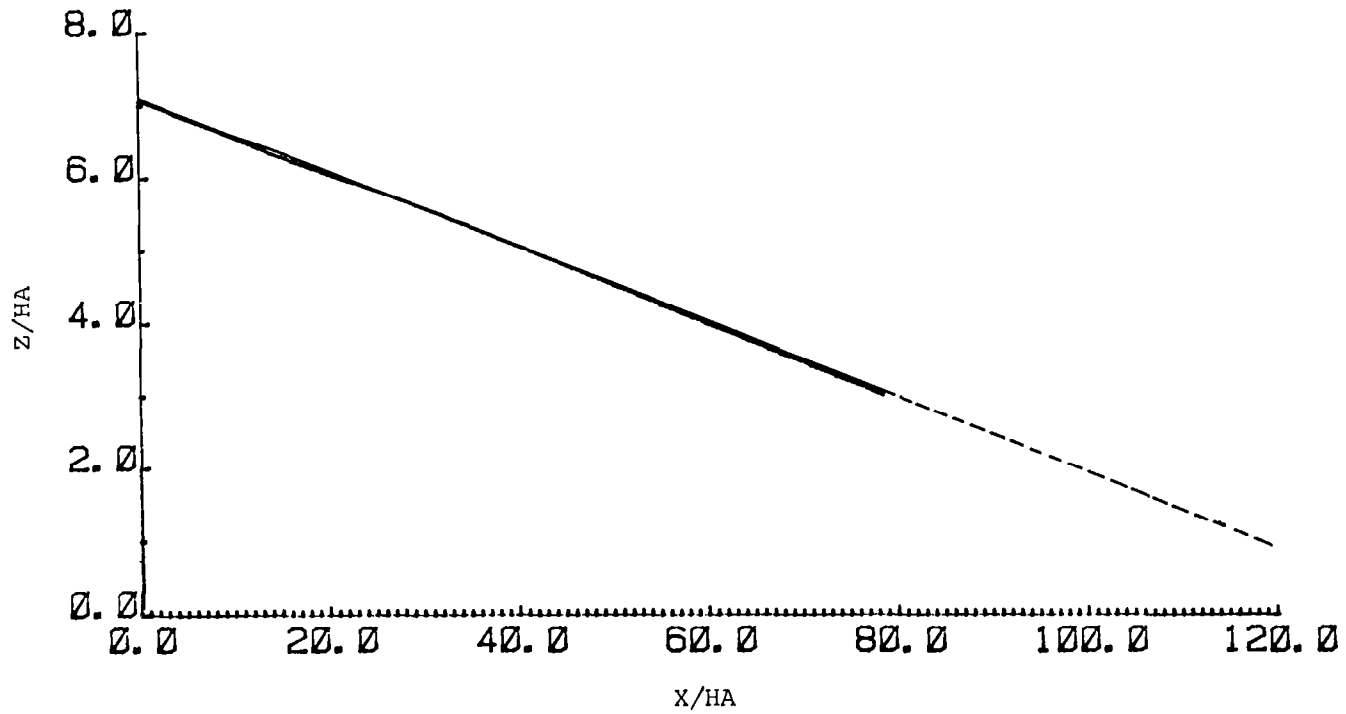amplitude sinusoidal wave at the phugoid frequency.

Figure 27   Simulated trajectory of a B727 under autopilot control flown
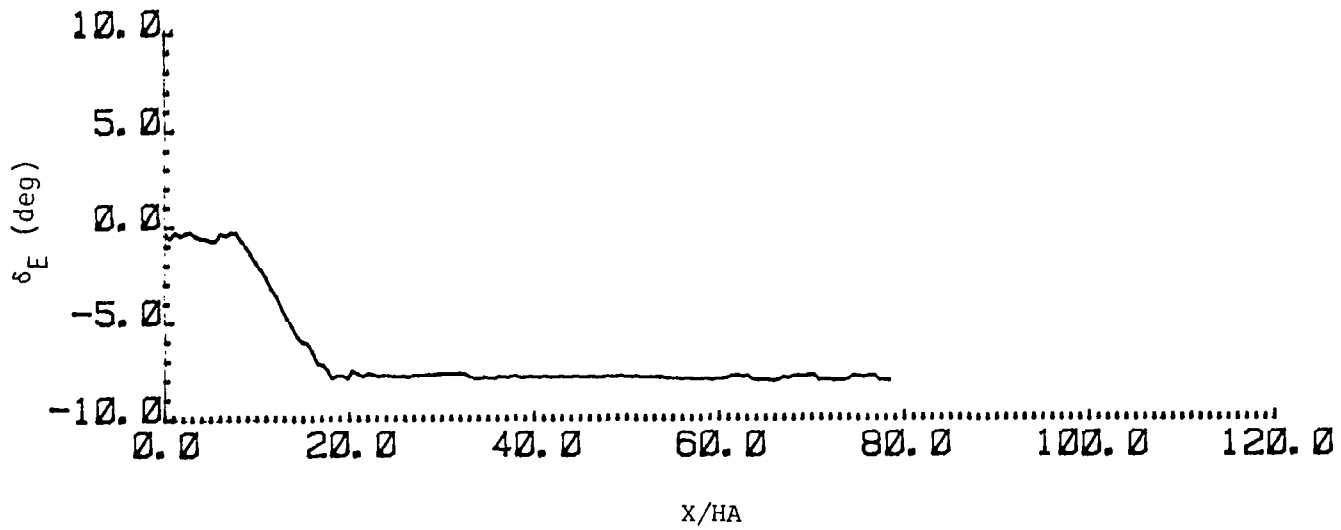through a 6 m/s amplitude phugoidal sine wave.

Figure 28   Autopilot elevator inputs to B727 in flight through a 6 m/s
amplitude phugoidal sine wave.
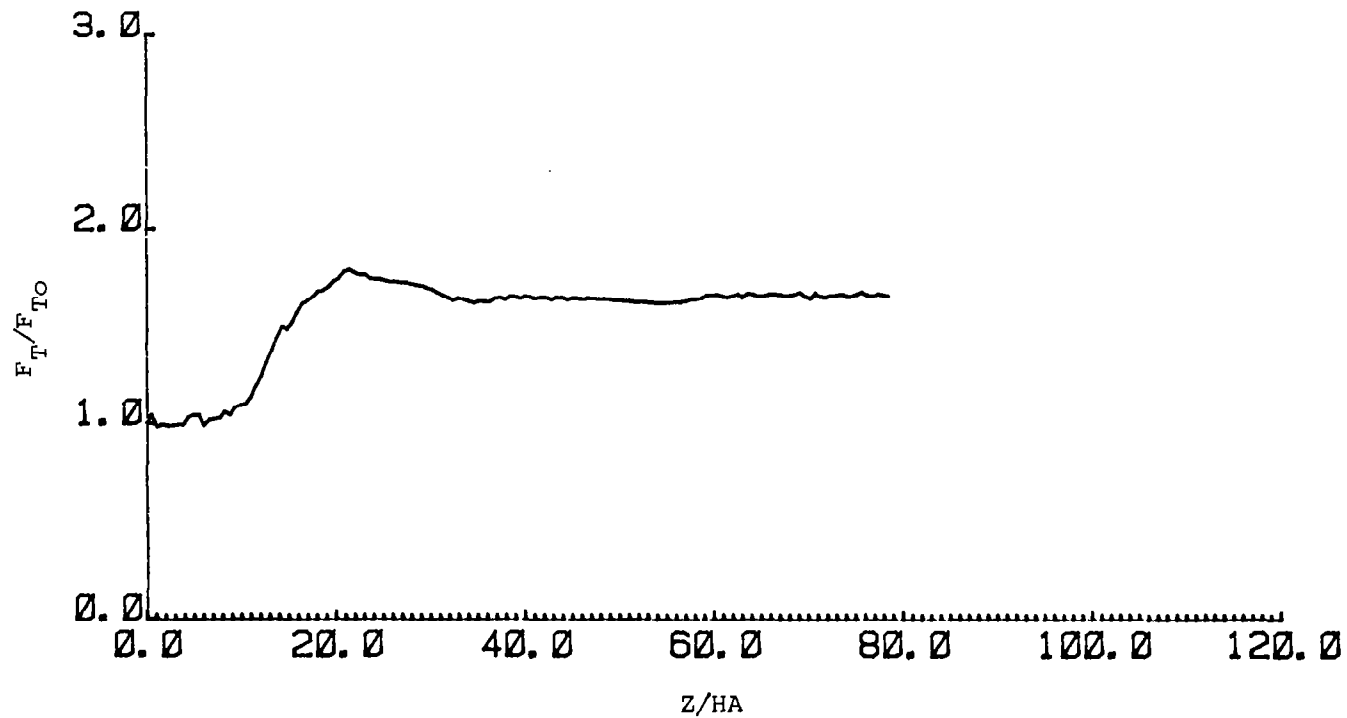
Figure 29 Autopilot thrust inputs to B727 in flight through a 6 m/s amplitude phugoidal sine wave.

disturbance, the oscillations of the fixed-stick case can be almost completely eliminated.

Simulated landings with pilots of various performance ratings were flown down the same sinusoidal wave. Figure 30 illustrates that a pilot with a 25 percent rating can easily negotiate the disturbance with only a slight dip below the glide slope. The wave-like "humps" in the elevator control setting (Figure 31), observed from X/HA = 0 to 4 and from X/HA = 35 to 80, represent pilot inputs to counter the aircraft's slight natural phugoidal oscillation in the steady 6 m/s head wind before the wave and in the tail wind after the wave, respectively.

Figure 32 shows the flight path of an aircraft controlled by a simulated pilot with a 5.5 percent performance rating. Passing through the shear wave, this pilot does not react quickly enough to the decreasing airspeed caused by the decreasing head wind, and the aircraft falls a maximum of 23 m below the glide slope. The pilot then regains control and applies step inputs to the elevator and throttle (Figures 33 and 34) to get back on the glide slope. In general, the pilot's approach is fairly good.

The results of this simulation show that a 6 m/s thunderstorm environment phugoid wave is not very severe from the standpoint of pilot control, as even a pilot with low performance capability can make the approach without too much deviation from the glide slope. However, had the deviation below the glide slope occurred relatively close to the runway threshold, the 5.5 percent rated pilot would have been forced to execute a go-around.

5.4 Simulated B727 Flight Through Sinusoidal 14 m/s Amplitude Wave Near Phugoid Frequency

In the following simulations, the B727 is flown through a longitudinal wave disturbance representative of a very strong thunderstorm cell wind profile. A 14 m/s amplitude wave is chosen based on longitudinal thunderstorm wind data analyzed by Frost, Camp, and Wang [10]. The aircraft is initially trimmed for flight in a steady 14 m/s head wind which
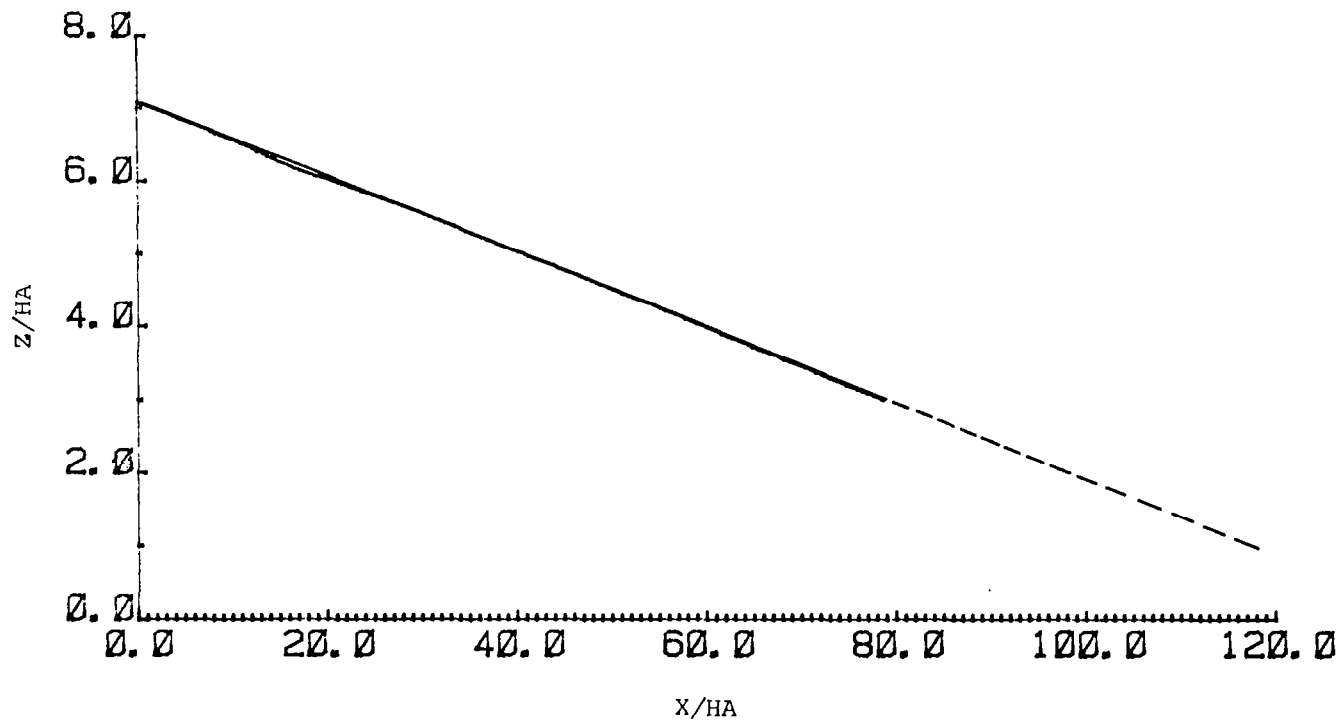
Figure 30   Simulated trajectory of a B727 controlled by a 25 percent rated
pilot flown through a 6 m/s amplitude phugoidal sine wave.

Figure 31   Elevator inputs by 25 percent rated pilot to B727 flown through a
6 m/s amplitude phugoidal sine wave.

Figure 32   Simulated trajectory of a B727 controlled by a 5.5 percent rated
pilot flown through a 6 m/s amplitude phugoidal sine wave.

10. 0
5. 0
0. 0
-5. 0
-10. 0

δ_E (deg)

0. 0   20. 0   40. 0   60. 0   80. 0   100. 0   120. 0

X/HA
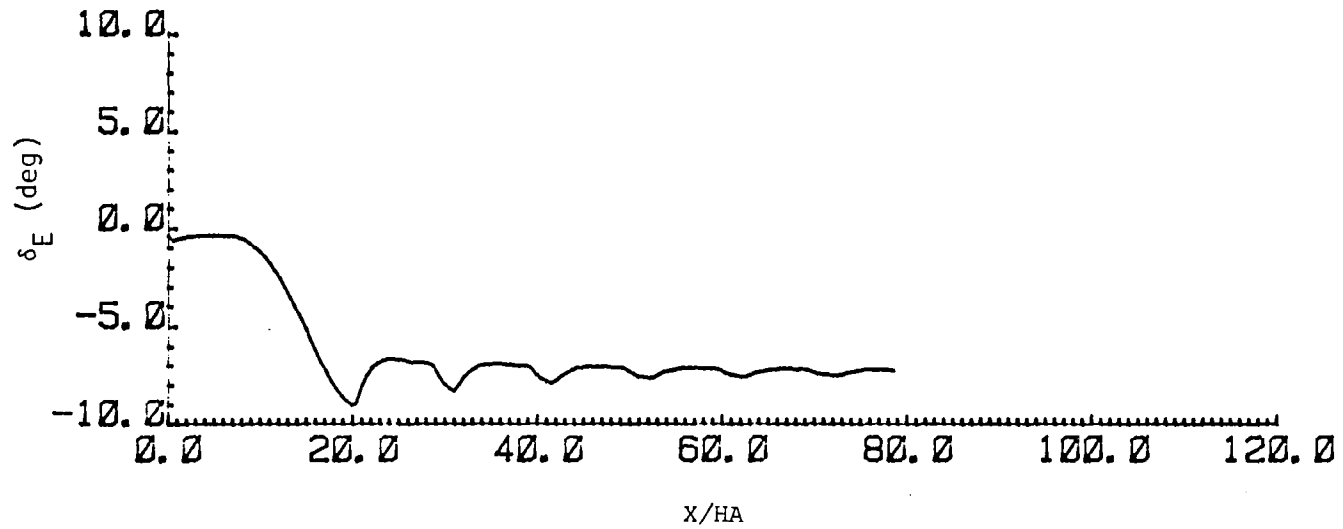
Figure 33   Elevator inputs by 5.5 percent rated pilot to B727 flown through a
6 m/s amplitude phugoidal sine wave.
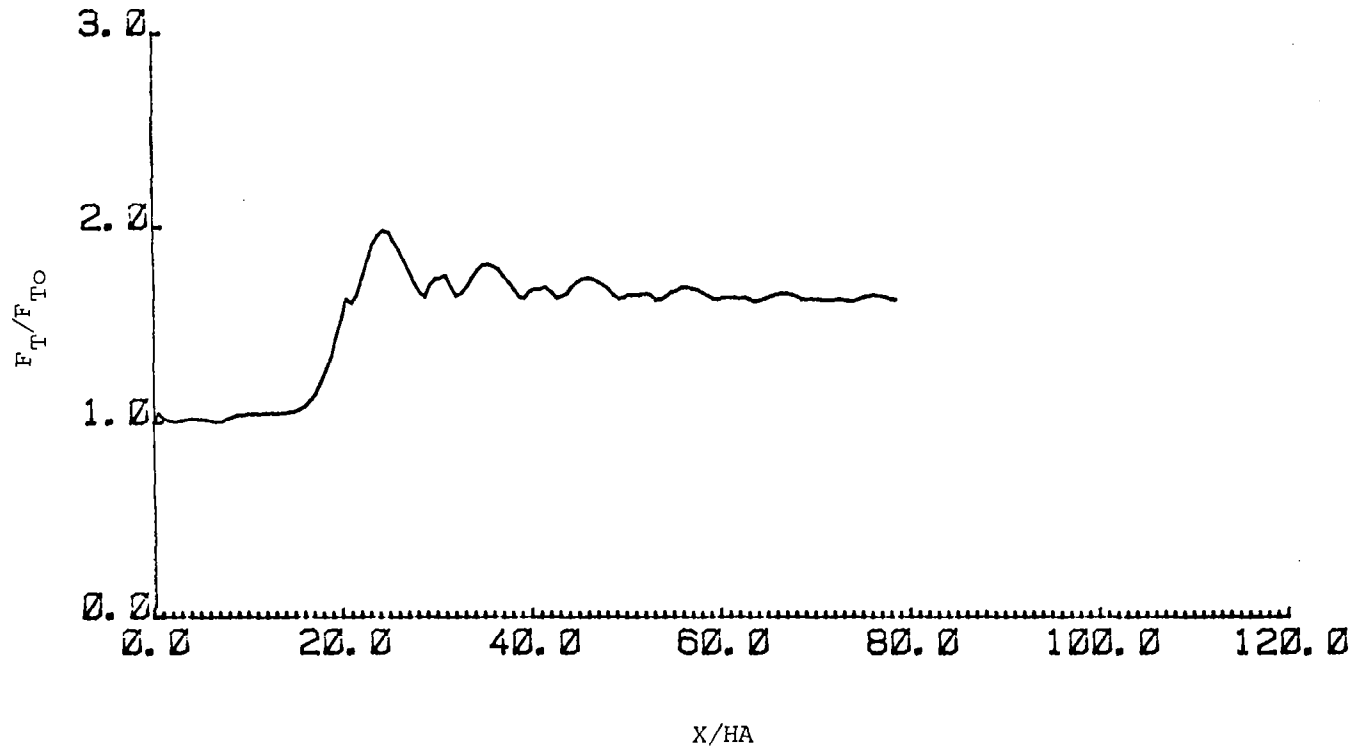
Figure 34 Thrust inputs by 5.5 percent rated pilot to B727 flown through a 6 m/s amplitude phugoidal sine wave.

shears as a wave at approximately the aircraft's phugoid frequency to a steady 14 m/s tail wind for the remainder of the run.

The simulated trajectory of an autopilot-controlled aircraft is shown in Figure 35. The aircraft encounters the decreasing head wind at approximately X/HA = 8 and begins to fall below the glide slope. The autopilot increases thrust (Figure 36) and moves the elevator to full negative deflection (Figure 37) to pitch the aircraft nose-up. The aircraft falls a maximum of 15 m below the glide slope until it responds to the added controls and pulls out of its descent at X/HA = 14. Due to the added controls, the aircraft ascends above the glide slope to a maximum of 23 m at X/HA = 30. The autopilot then decreases thrust to allow the aircraft to gradually fall back and recapture the glide slope and finish with a near perfect approach. While it is unlikely that an aircraft would execute an approach in a 14 m/s tail wind, note that the autopilot trims the aircraft with full nose-up elevator deflection and twice the initial thrust to maintain flight in this tail wind.

Figure 38 shows the simulated trajectory of an aircraft controlled by a pilot with a performance rating of 50 percent. The aircraft drops approximately 18 m below the glide slope when it encounters the decreasing head wind. Again, thrust is increased (Figure 39) and elevator angle is increased to full nose-up deflection (Figure 40) to counter the effect of the decreasing airspeed. However, due to the farther drop below the glide slope and slower response time of the pilot as compared with the auto-pilot, the aircraft does not rise as high above the glide slope as it did under autopilot control. Thrust is then decreased so that the aircraft can descend to intercept the glide slope and maintain an excellent approach through the remaining tail wind.

The flight profile and control inputs of an aircraft controlled by a 25 percent rated pilot (Figures 41 through 43) are examined next. During the encounter with the shear wave, the aircraft falls a maximum of 23 m below the glide slope. This would obviously create a hazardous situation had the aircraft encountered such a wave in the immediate vicinity of the runway threshold. Because of the large drop below the glide slope and slow response of the pilot, the aircraft rises only slightly above the
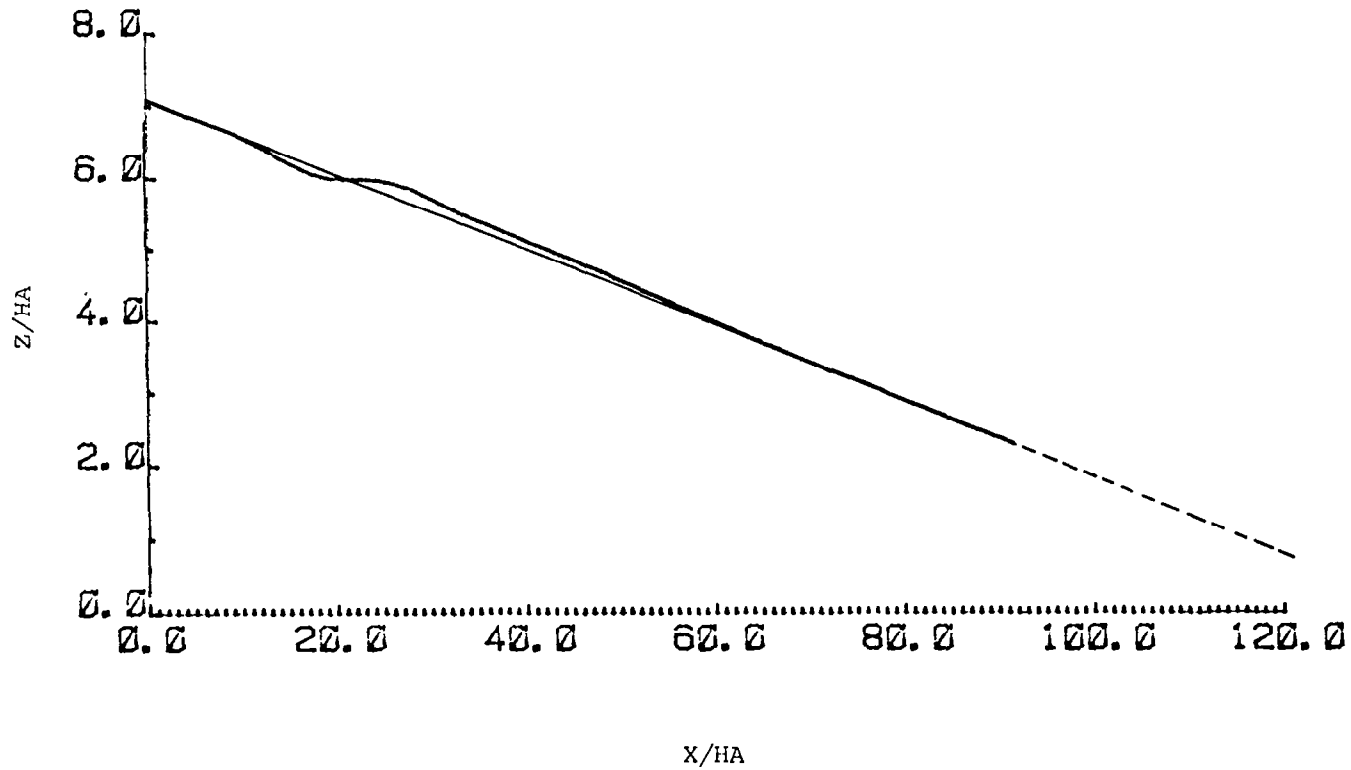
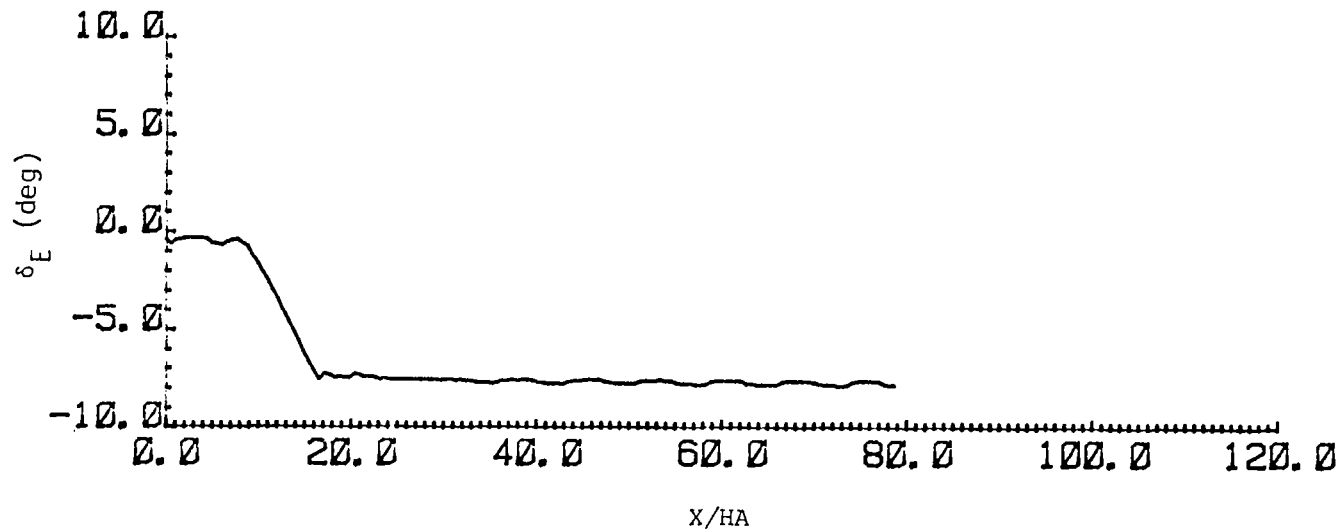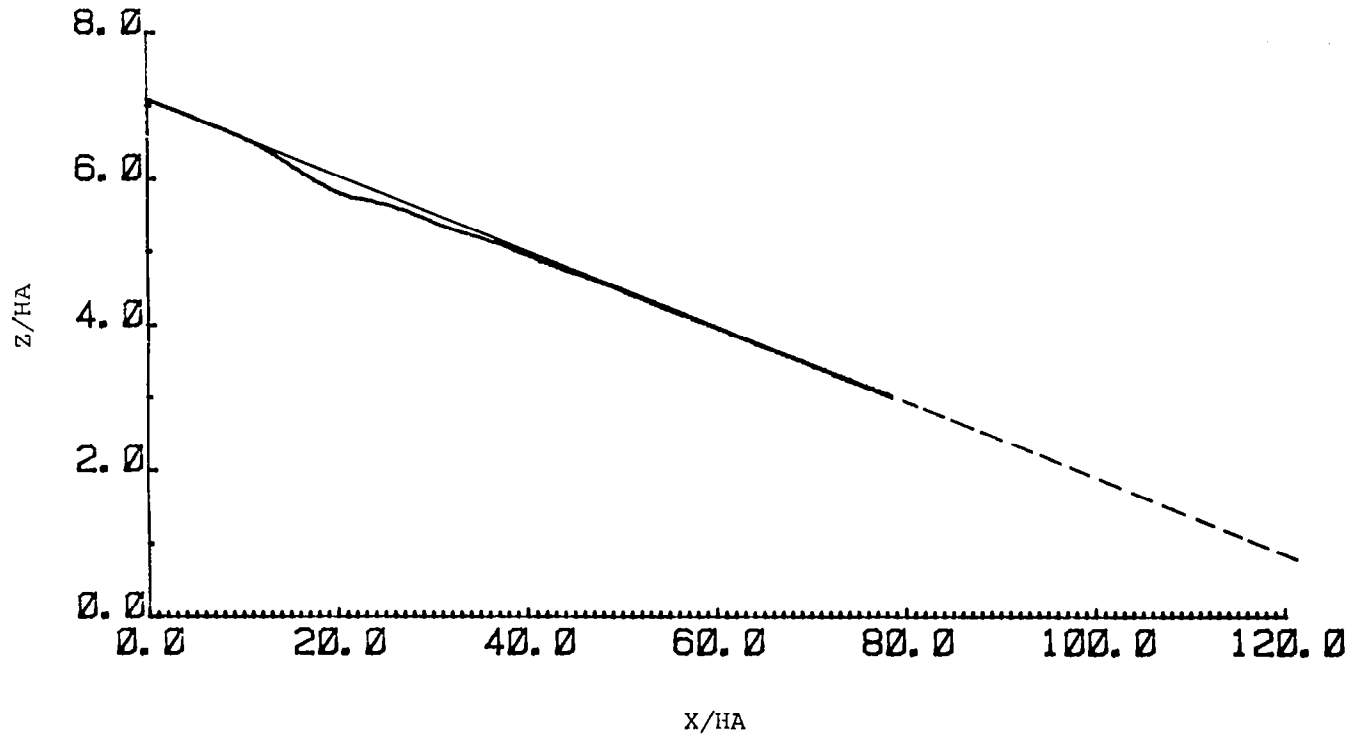Figure 35 Simulated trajectory of a B727 under autopilot control flown
through a 14 m/s amplitude phugoidal sine wave.
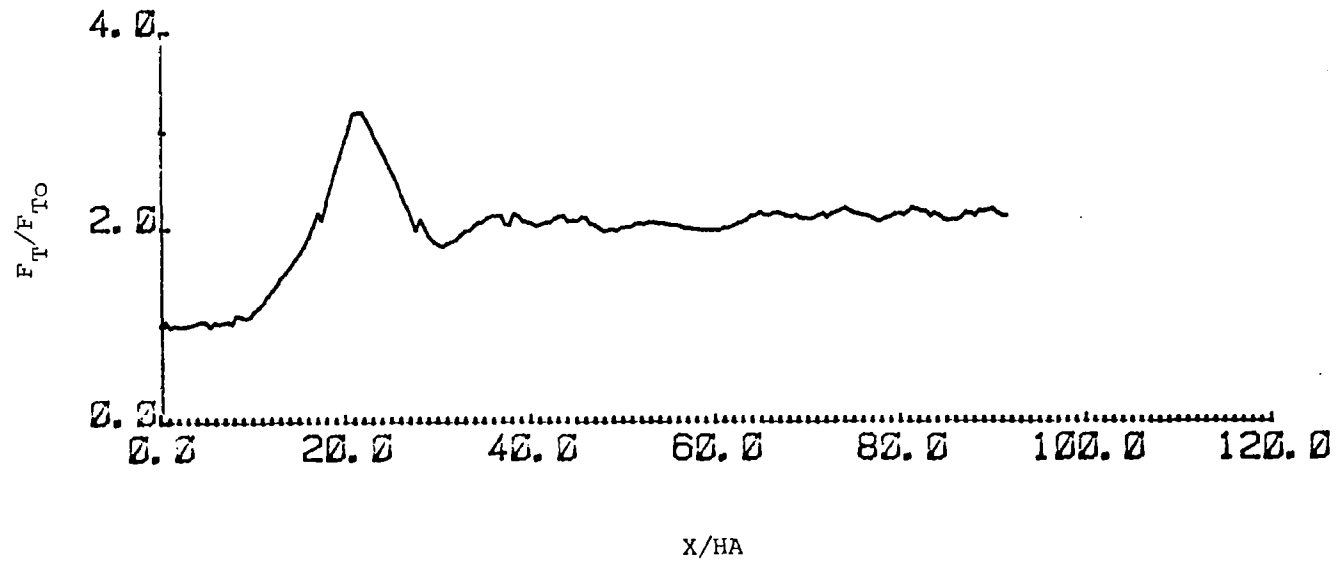
Figure 36   Autopilot thrust inputs to B727 in flight through a 14 m/s
amplitude phugoidal sine wave.
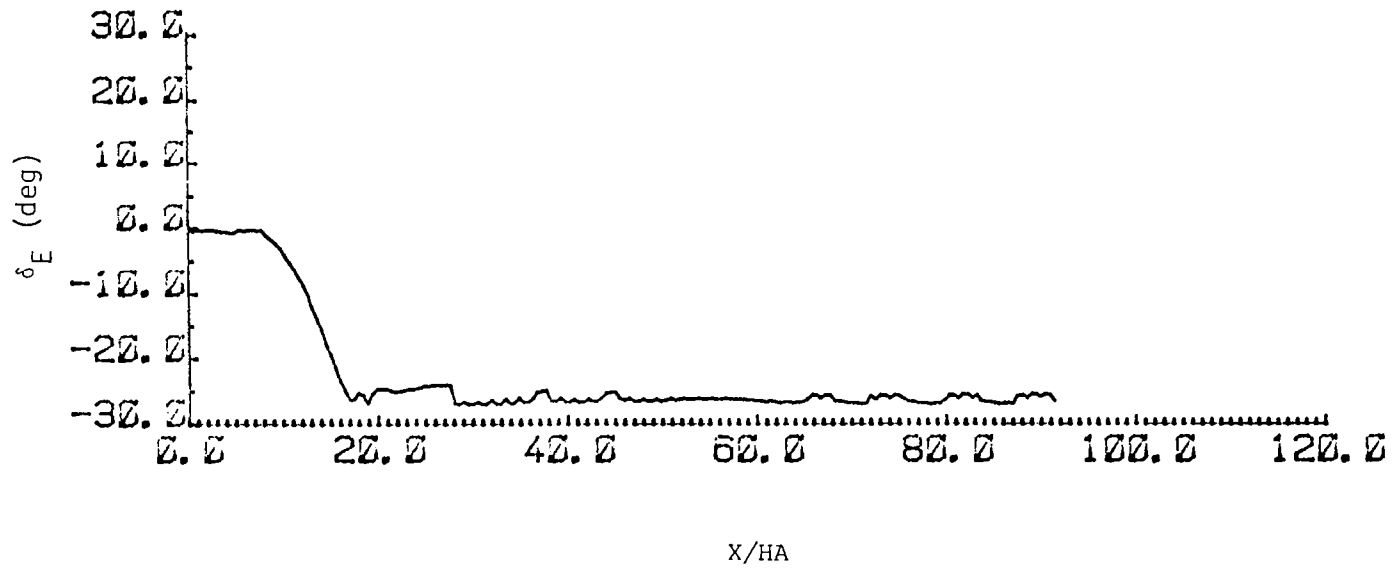
Figure 37   Autopilot elevator inputs to B727 in flight through a 14 m/s amplitude phugoidal sine wave.

Figure 38 Simulated trajectory of a B727 controlled by a 50 percent rated
          pilot flown through a 14 m/s amplitude phugoidal sine wave.

Figure 39   Thrust inputs by a 50 percent rated pilot to B727 flown through
a 14 m/s amplitude phugoidal sine wave.

X/HA

Figure 40 Elevator inputs by a 50 percent rated pilot to B727 flown
through a 14 m/s amplitude phugoidal sine wave.

Figure 41   Simulated trajectory of a B727 controlled by a 25 percent rated
pilot flown through a 14 m/s amplitude phugoidal sine wave.

Figure 42 Elevator inputs by a 25 percent rated pilot to B727 flown through a 14 m/s amplitude phugoidal sine wave.

Figure 43 Thrust inputs by a 25 percent rated pilot to B727 flown
through a 14 m/s amplitude phugoidal sine wave.

glide slope as it pulls out of its descent. Thrust is decreased at X/HA = 21 to return the aircraft to the glide slope where it remains for the length of the run.

Finally, the performance of a 5 percent rated pilot in an aircraft encountering the 14 m/s shear wave is examined. Figures 44, 45, and 46 show the flight profile and the elevator and thrust inputs, respectively. As the aircraft enters the decreasing head wind, the airspeed decreases and the aircraft begins to descend. The pilot's response is extremely slow, allowing a very high sink rate to build up. Because of the large lag on the controls and severe change in the wind, control of the aircraft is lost. The initial loss of control builds up to the point where the control loop starts to decrease thrust between X/HA = 13 to X/HA = 17 (Figure 46). At this point there appears to be a small "bug" in the control loop. The thrust should not decrease with increasing sink rate even though the aircraft is experiencing an increasing speed.

It is believed that a small correction to the gain on the vertical velocity deviation in the pitch control variable θ_c, which has been kept constant for all previous cases, will correct this slight anomaly. However, the severity of this wind field and the low performance rating used in this case is apparently responsible for this effect. The proper setting of this gain will require further investigation. Nevertheless, the aircraft does eventually begin to regain thrust control and pull out of its descent at approximately X/HA = 18 when the vertical velocity peaks, compensating for the low gain. Thrust is eventually increased to a higher setting (Figure 46) and step inputs are made to both elevator and thrust to return the aircraft to the glide slope. The response of the aircraft to the step inputs is shown by the wave-like trajectory in Figure 44 from X/HA = 20 to X/HA = 75.

The results of this simulation illustrate the severity of strong thunderstorm-related shear in the horizontal wind. The autopiloted and 50 percent rated pilot-controlled aircraft maintained fairly good approaches but not without significant deviation below the glide slope. The 25 percent rated pilot-controlled aircraft experienced a fairly large drop below the glide slope of such magnitude that a go-around would have had to

Figure 44   Simulated trajectory of a B727 controlled by a 5 percent rated
pilot flown through a 14 m/s amplitude phugoidal sine wave.

X/HA
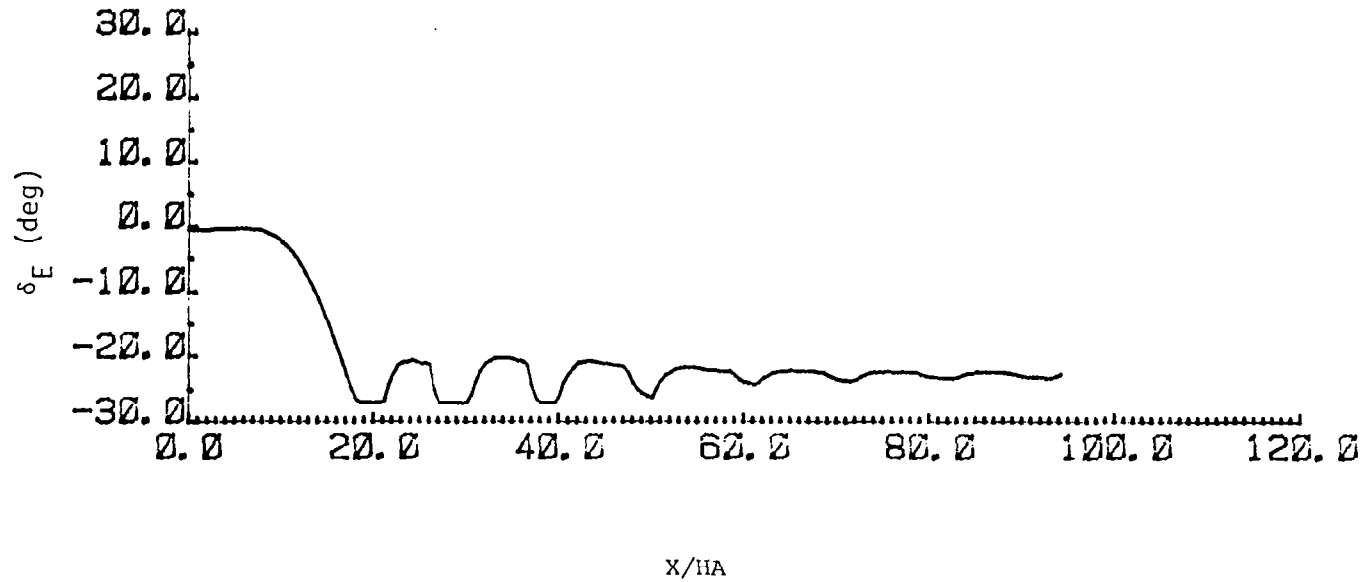
Figure 45   Elevator inputs by a 5 percent rated pilot to B727 flown
through a 14 m/s amplitude phugoidal sine wave.

X/HA

Figure 46   Thrust inputs by a 5 percent rated pilot to B727 flown through
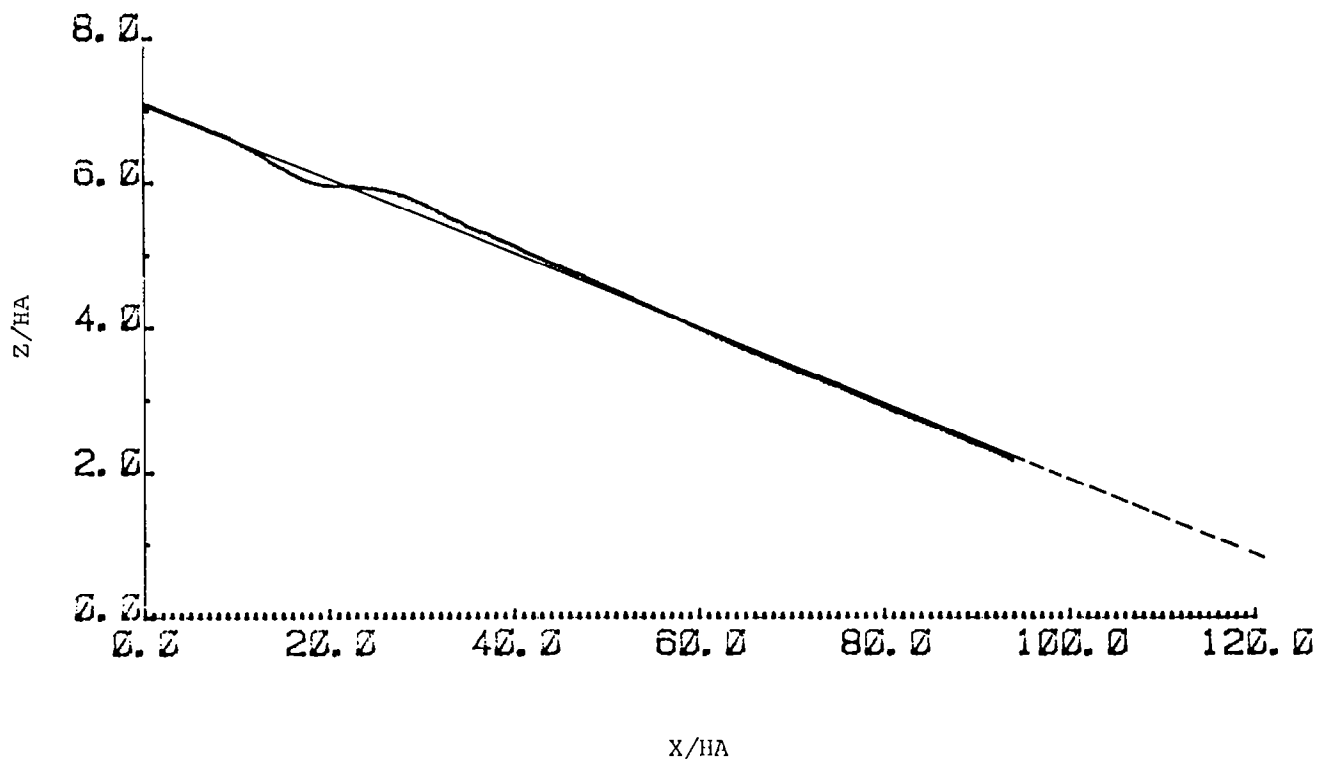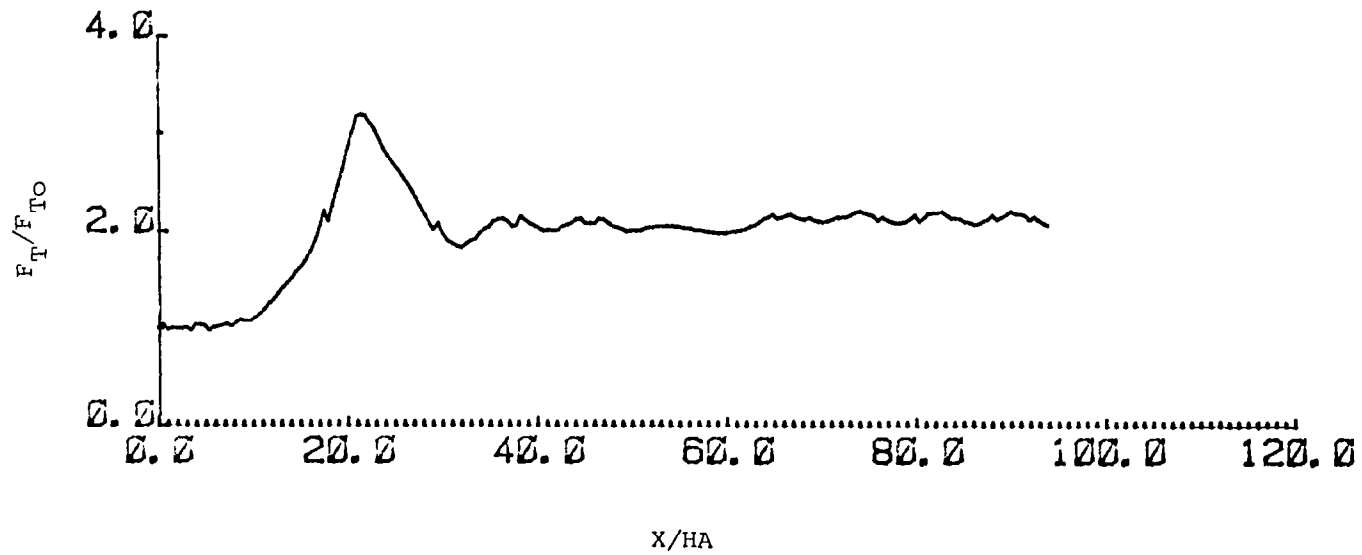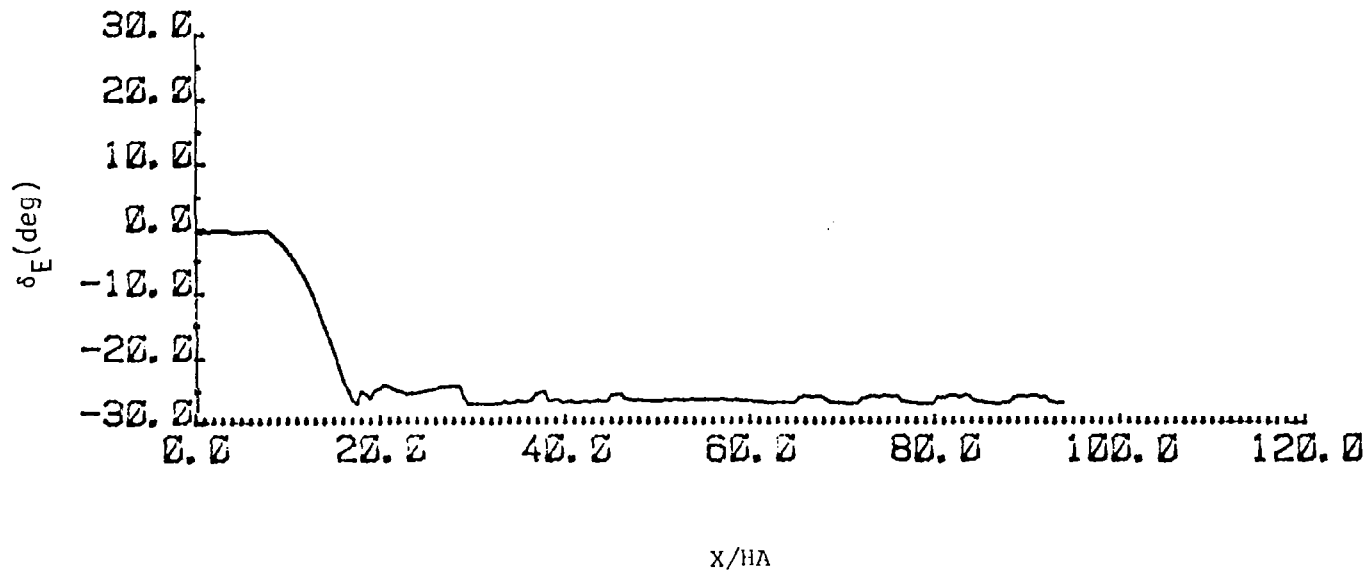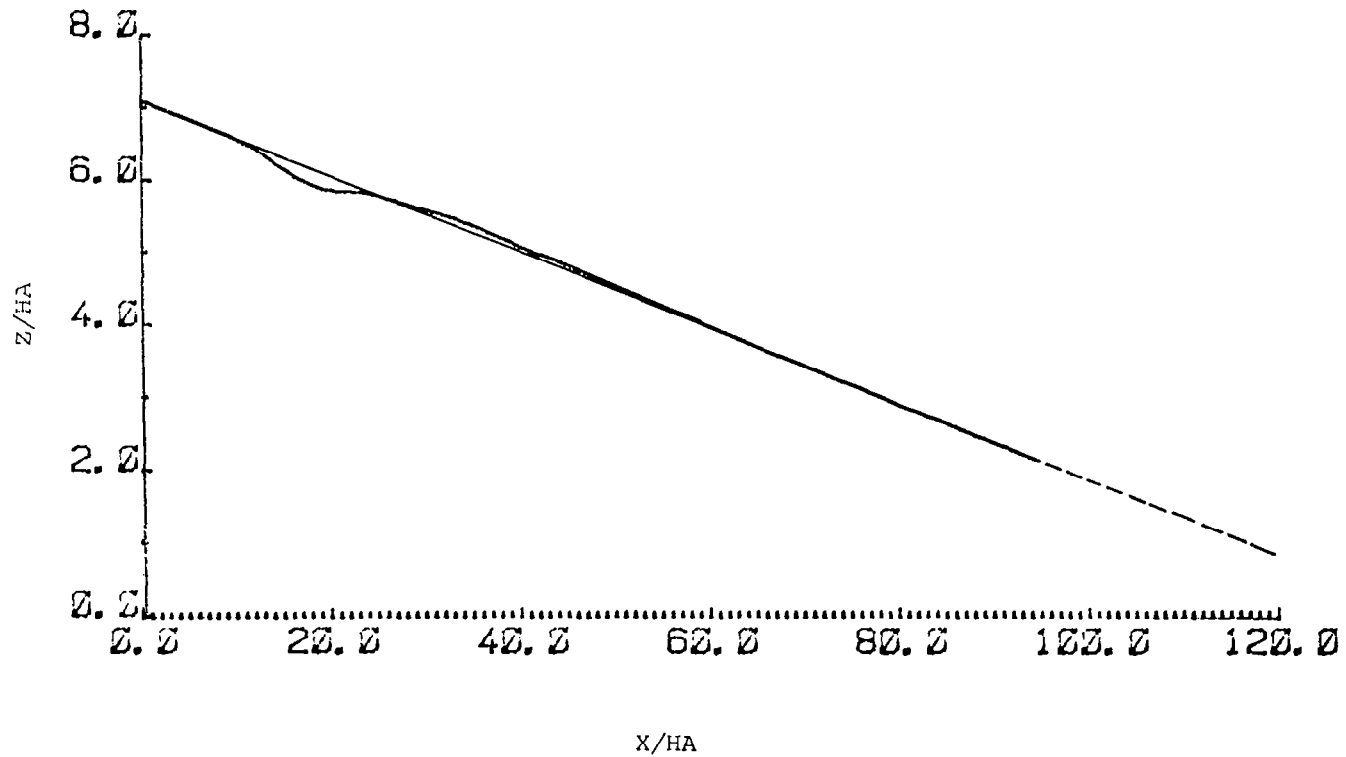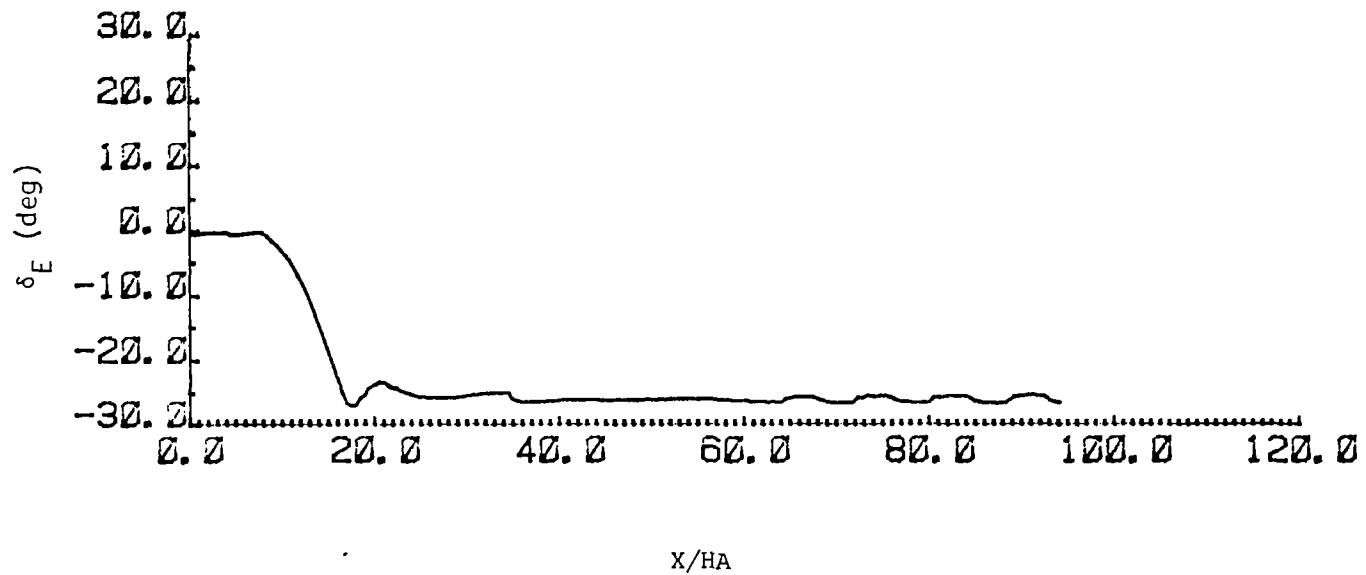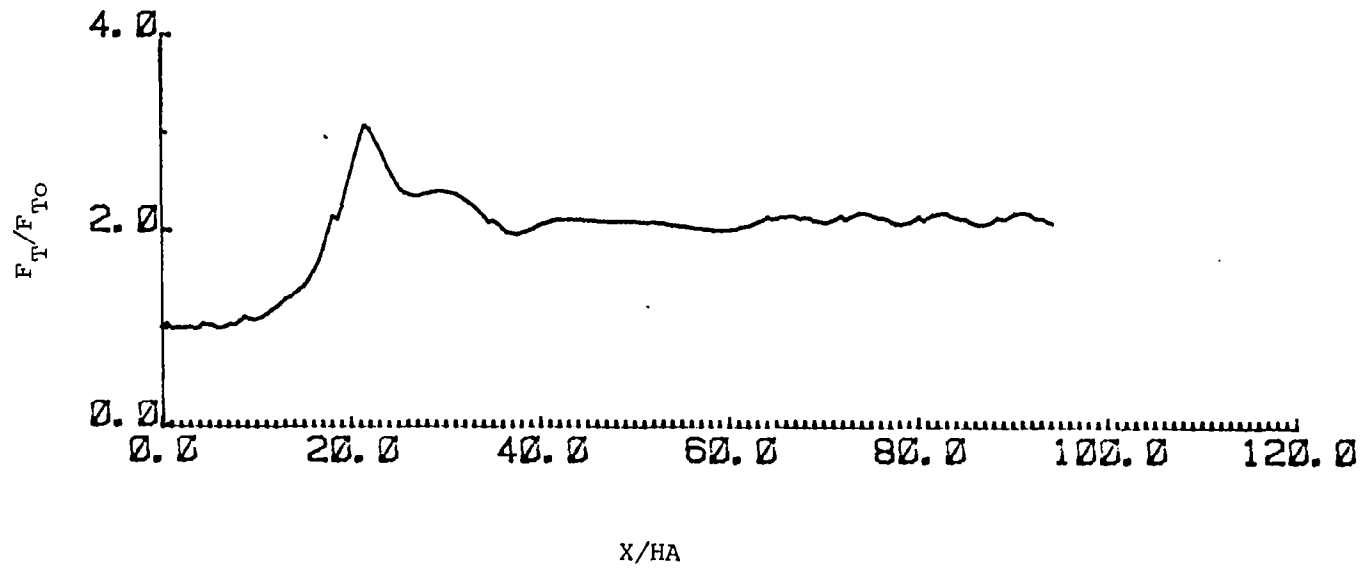a 14 m/s amplitude phugoidal sine wave.

be executed had the shear wave been encountered relatively close to the runway threshold. Finally, the inability of the low performance 5 percent rated pilot to negotiate the high rate of descent caused by the shear wave shows the danger of slow response and failure to properly recognize the effects of wind shear on approach.

5.5 Simulated B727 Flight Through Full Sinusoidal 10 m/s Amplitude Wave Near Phugoid Frequency

In the final simulations the B727 is flown through a full 10 m/s head wind to tail wind sinusoidal phugoid frequency wave. The wind increases from 0 m/s to become a 10 m/s head wind which shears to a 10 m/s tail wind and then returns to zero wind for the remainder of the run.

Figure 47 shows the trajectory of a simulated B727 under autopilot control flown through the sinusoidal wind field. The aircraft is forced slightly above the glide slope when it encounters the increasing head wind and drops slightly below the glide slope as it enters the increasing tail wind. The aircraft then rises above the glide slope as the tail wind diminishes to 0 m/s. The autopilot eventually returns the aircraft to the glide slope to land on target.

Figures 48, 49, and 50 show the simulated flight path, elevator inputs, and thrust control inputs, respectively, for a piloted B727 flown through the phugoidal sine wave. The pilot model used for this run was based on the data for pilot A from Adams and Bergeron [7] (Table 1). This pilot was rated relatively high based on high static gains, high lead time constants, and low lag time constants. The aircraft rises above the glide slope when encountering the increasing head wind. The pilot cuts thrust to zero and pitches the nose down to counteract the rise above the glide slope. The aircraft then encounters the head wind to tail wind shear and drops below the glide slope, due to the previously decreased power, necessitating a thrust increase and pitch-up of the nose. Eventually, the aircraft is brought back to the glide slope and retrimmed for the zero wind condition for a safe landing.

69
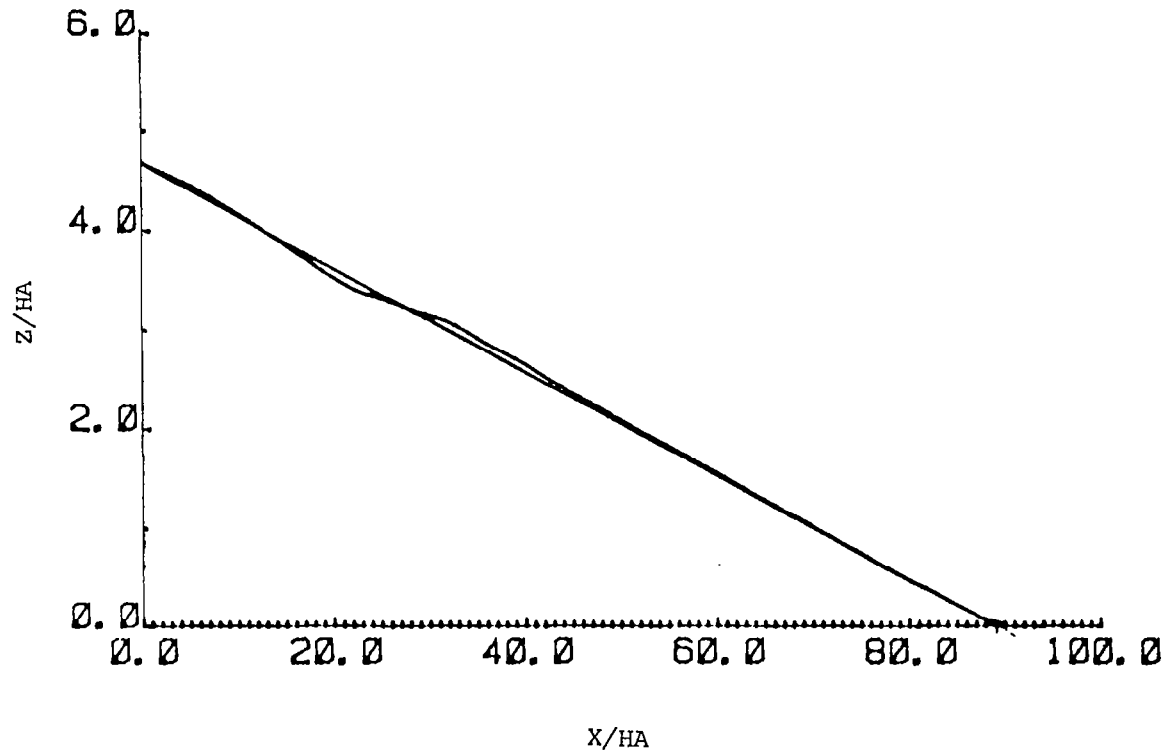
Figure 47   Simulated trajectory of an autopilot-controlled B727 through 10 m/s
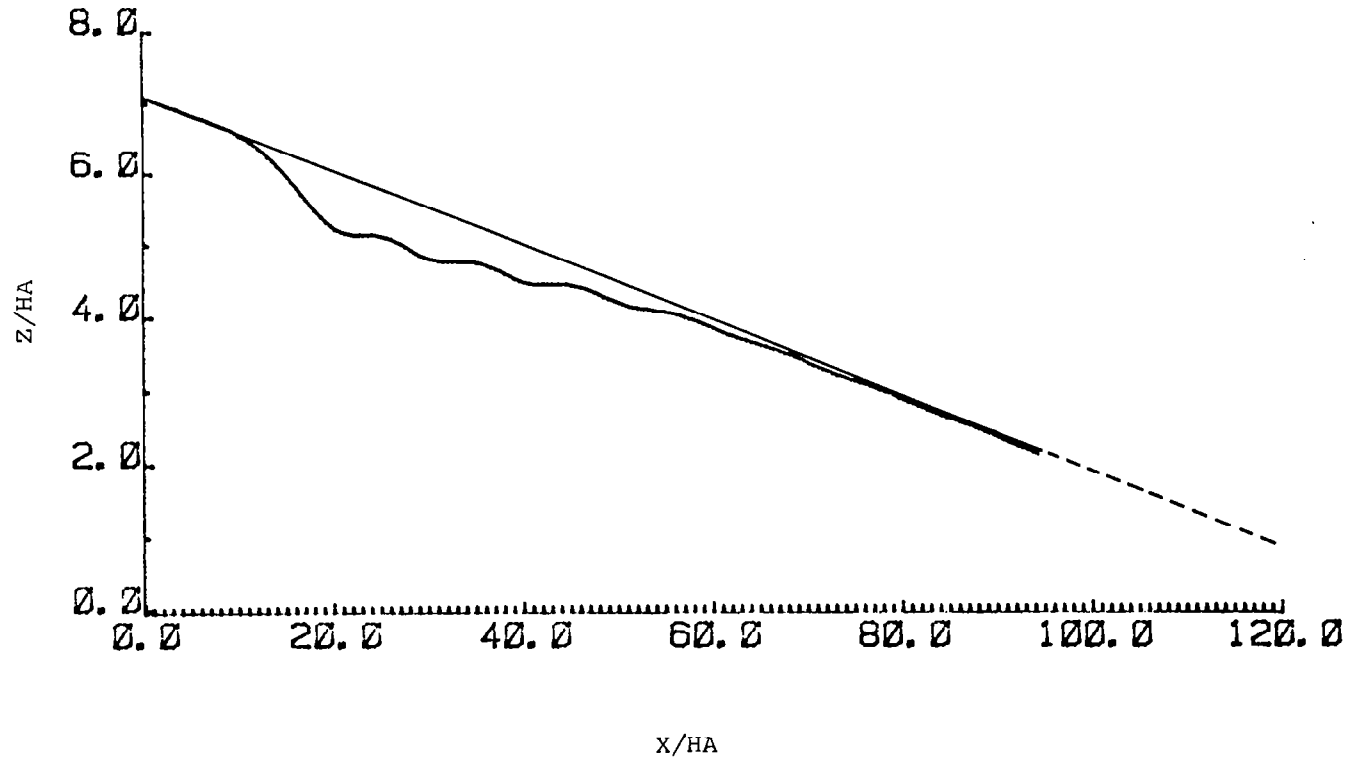amplitude phugoidal sine wave.

Figure 48   Simulated trajectory of a B727 controlled by pilot A flown through 10 m/s amplitude phugoidal sine wave.
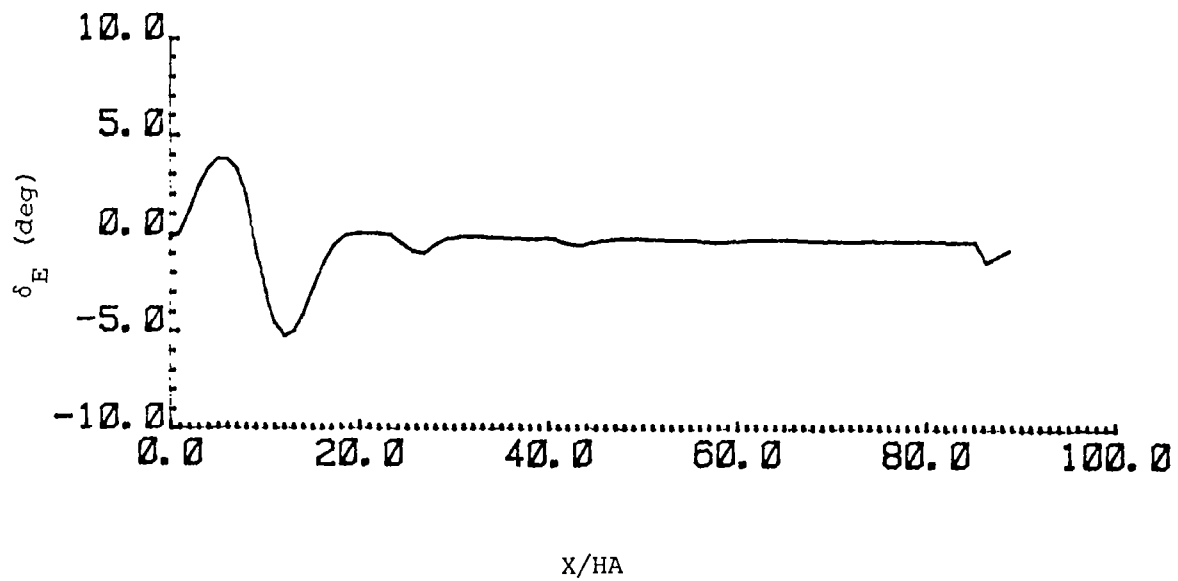
Figure 49   Elevator inputs by pilot A to B727 flown through 10 m/s amplitude
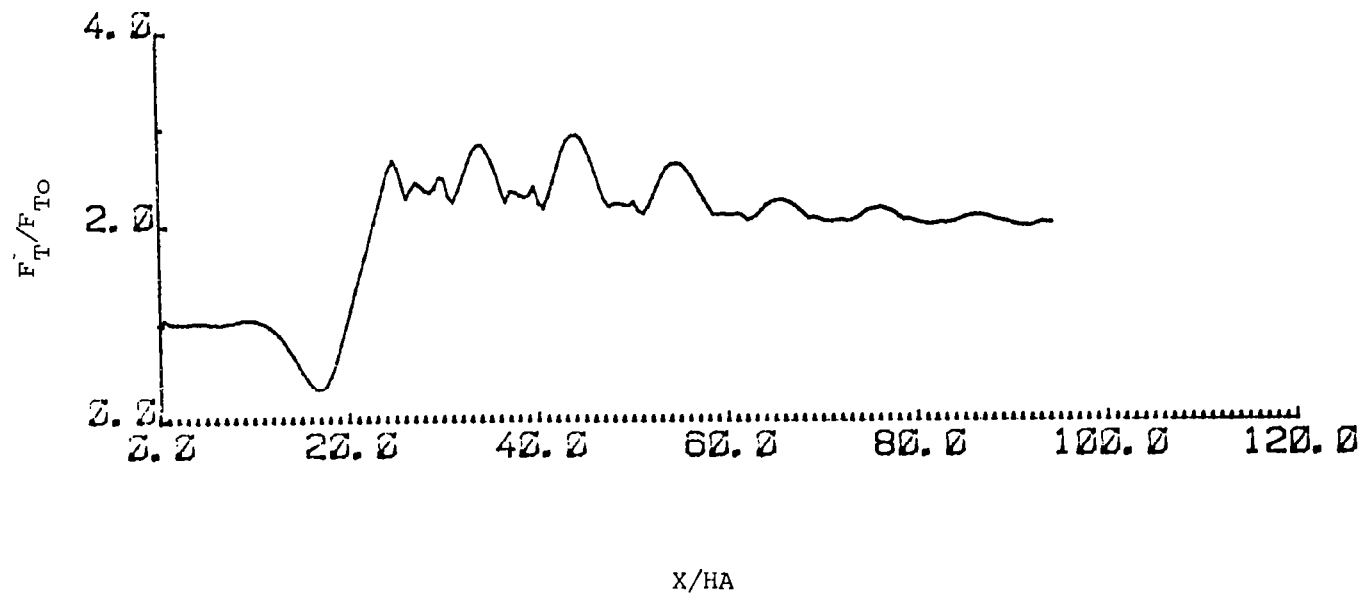   phugoidal sine wave.
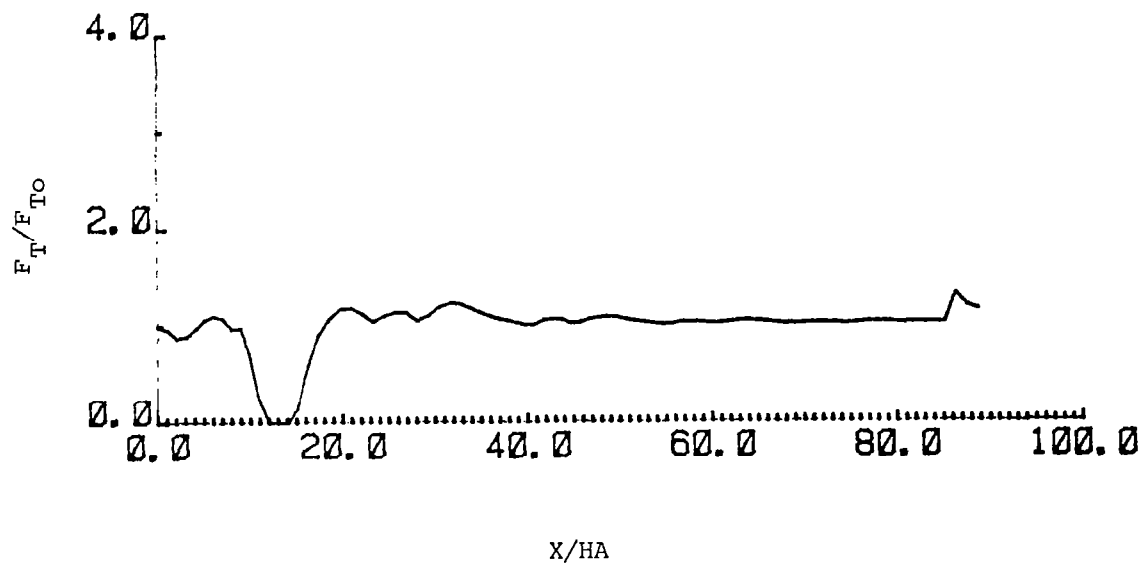
Figure 50   Thrust inputs by pilot A to B727 flown through 10 m/s amplitude phugoidal sine wave.

Figure 51 shows the trajectory of a simulated B727 flown through the shear wave by pilot F. As shown from the data of Adams and Bergeron [7] in Table 1, this pilot is of relatively low skill due to a low static gain, low lead time constant, and high lag time constant. The aircraft as controlled by this pilot rises highest above the glide slope and drops farthest below the glide slope due to higher response lag time. The pilot is unable to bring the aircraft back to the glide slope and lands short. The wave-like humps in the trajectory represent attempts to stabilize the approach angle.

This simulation compares the relative degrees of control applied to an aircraft landing through a phugoidal shear wave. The optimization autopilot rapidly corrects for the wind changes with low lag time and maintains the tightest control. Pilot A possesses higher lag than the autopilot and illustrates the danger of decreasing thrust when encountering a head wind to tail wind shear. The aircraft dropped below the glide slope but the pilot was able to regain control and recover the approach. The lower skilled, higher lagged pilot F was unable to safely counter the shear and landed short.
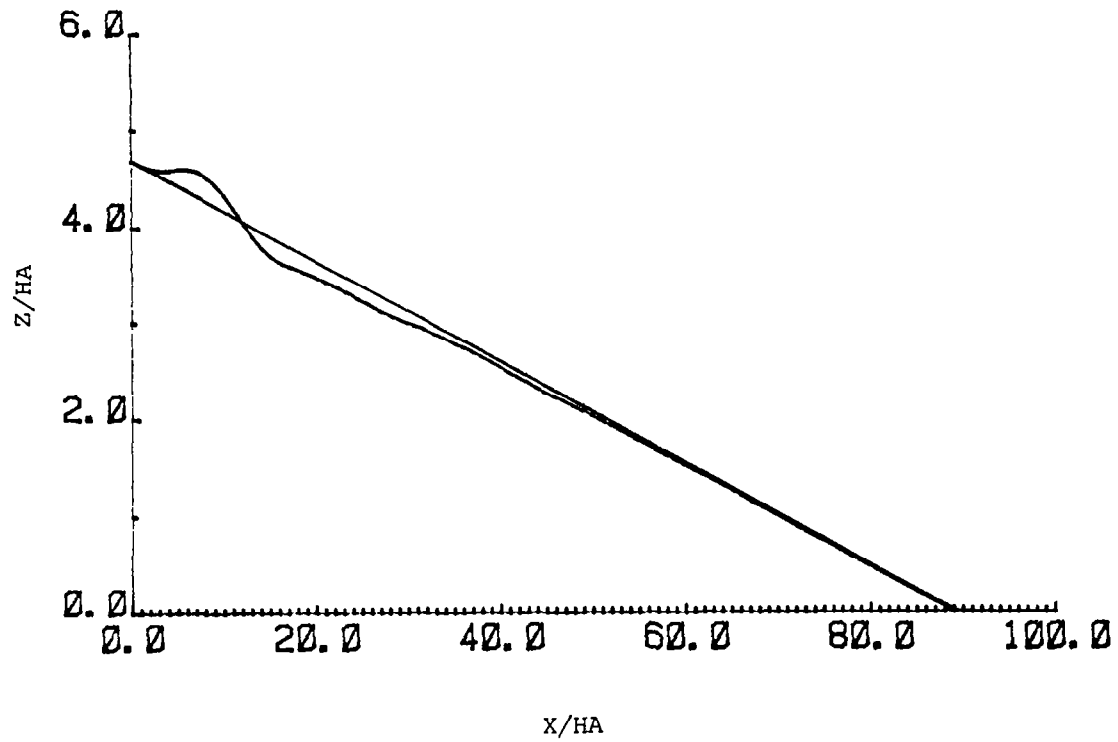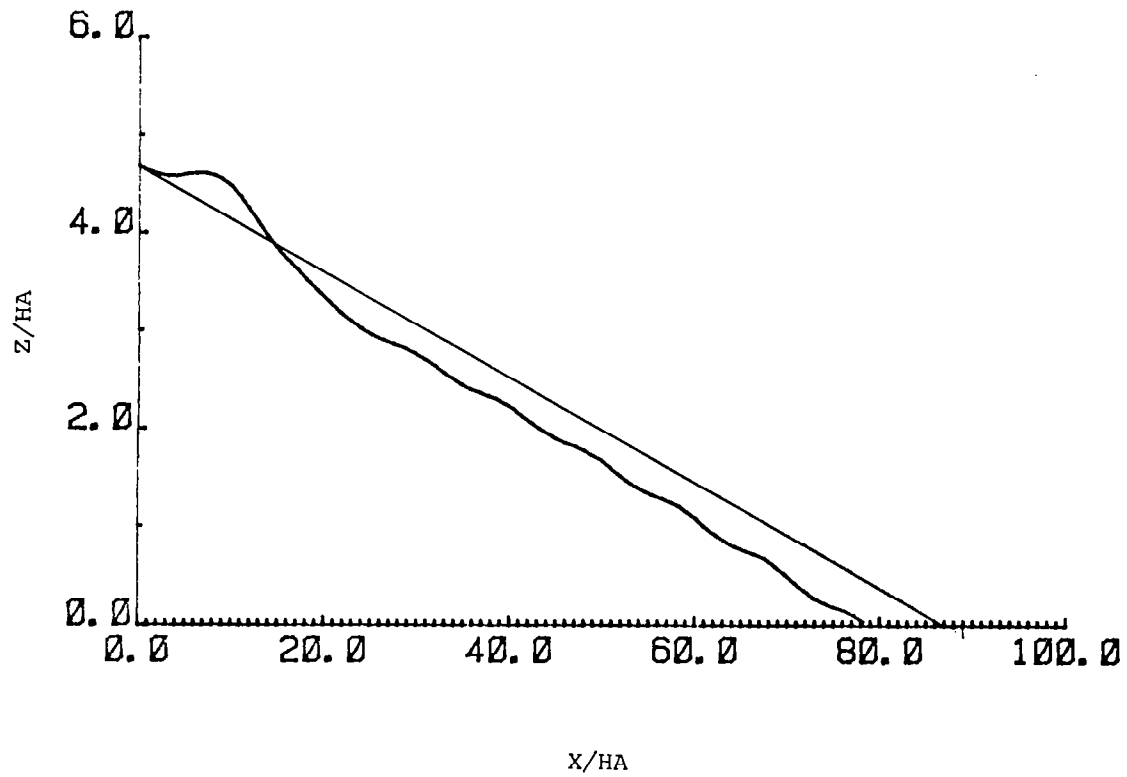
Figure 51   Simulated trajectory of a B727 controlled by pilot F flown through
10 m/s amplitude phugoidal sine wave.

6.0 CONCLUSIONS

The purpose of this study was to evaluate the response of the pilot-aircraft system to wind shear. This was carried out by performing a parametric study of pilot performance rating and by use of actual pilot data. Performance ratings ranged between 100 percent autopilot control (perfect pilot) and "hands off" or 0 percent control (fixed-stick), with the human pilot having any performance rating in this range. Fixed-stick, autopilot, and manned performance of both a simulated B727, a medium-sized commercial transport, and a simulated Queen Air, a small commuter-type aircraft, flown through a glide slope longitudinal wind profile detected by Doppler radar were compared. The wave-form wind disturbance was shown to excite the phugoid oscillations of both aircraft when flown in the fixed-stick mode but presented no control problems for manned aircraft. The fixed-stick simulations also showed agreement with the theories of McCarthy, Blick, and Bensch [3] and Frost and Crosby [4] stating that the oscillatory effects of a shear wave are greater on transport aircraft than on smaller aircraft as predicted by aircraft stability theory.

A simulation was also carried out flying the fixed-stick, autopilot controlled, and manned aircraft with characteristics of a B727 through a 6 m/s amplitude head wind to tail wind phugoid frequency shear wave representative of the thunderstorm cell wind environment. This case also revealed phugoid oscillations but clearly illustrated that this shear wave was not a serious problem to a manned vehicle.

However, in the stronger disturbance of a 14 m/s head wind to tail wind phugoid frequency shear wave, significant deviation from the glide slope was noted for the autopilot, 50 percent rated pilot, and 25 percent rated pilot flight simulations. The low performance, 5 percent rated pilot initially lost control of the aircraft and dropped farthest below the glide slope. However, thrust was eventually increased to bring the aircraft back up to the glide slope.

76

In flight simulations through a full 10 m/s phugoidal sine wave, comparisons were made between autopilot control and control by simulated pilots of varying skill. The autopiloted aircraft executed the best approach, while the high-skilled pilot descended below the glide slope but was eventually able to bring the aircraft back onto the glide path. However, the low-skilled pilot could not maintain adequate control and landed short.

The four wind profiles utilized in this study do not by any means limit the severity or variety of conditions to be found in the atmosphere. However, this research provides a better understanding of pilot-aircraft response to longitudinal wind shear and serves as an important input toward the development of a Doppler radar wind shear warning and detection system.

7.0 REFERENCES

1. National Transportation Safety Board. "Eastern Airlines, Inc., Boeing 727-225, John F. Kennedy International Airport, Jamaica, New York, June 24, 1975," Aircraft Accident Report No. NTSB-AAR-76-8, National Transportation Safety Board, Washington, D.C., March 12, 1976.

2. National Transportation Safety Board. "Eastern Airlines, Inc., Boeing 727-25, Atlanta Hartsfield International Airport, Atlanta, Georgia, August 22, 1979," Aircraft Incident Report No. NTSB-AAR-80-6, National Transportation Safety Board, Washington, D.C., May 28, 1980.

3. McCarthy, J., E. F. Blick, and R. R. Bensch. "Jet Transport Performance in Thunderstorm Wind Shear Conditions," NASA CR 3207, December, 1979.

4. Frost, W., and W. A. Crosby. "Investigations of Simulated Aircraft Flight Through Thunderstorm Outflows," NASA CR 3052, September, 1978.

5. Frost, W., and K. R. Reddy. "Investigations of Aircraft Landing in Variable Wind Fields," NASA CR 3073, December, 1978.

6. Dickinson, B. Aircraft Stability and Control for Pilots and Engineers. London: Sir Isaac Pitman and Sons, Ltd., 1968.

7. Adams, J. J., and H. P. Bergeron. "Measured Variation in the Transfer Function of a Human Pilot in Single Axis Tasks," NASA TN D-1952, October, 1963.

8. Neuman, F., and J. Foster. "Investigation of a Digital Automatic Aircraft Landing System in Turbulence," NASA TN D-6066, October, 1970.

9. Etkin, B. Dynamics of Atmospheric Flight. New York: John Wiley and Sons, Inc., 1972.

10. Frost, W., D. W. Camp, and S. T. Wang. "Wind Shear Modeling for Aircraft Hazard Definition," FAA-RD-78-3, February, 1978.

APPENDICES

APPENDIX A

DERIVATION OF THRUST AND ELEVATOR ANGLE CONTROL FUNCTIONS (F_T, δ_E)

The three degrees of freedom of the two-dimensional aircraft motion model are given by the following equations from Frost and Crosby [2]

$$\dot{q} = D_7 F_T + D_5 V_a^2 C_m \tag{1}$$

$$\dot{\gamma} V = D_6 \sin(\delta_T + \alpha) F_T - D_2 \cos\gamma + D_1 V_a^2 (C_L \cos\delta - C_D \sin\delta) \tag{2}$$

$$\dot{V} = D_6 \cos(\delta_T + \alpha) F_T - D_2 \sin\gamma - D_1 V_a^2 (C_L \sin\delta + C_D \cos\delta) \tag{3}$$

Equations 1, 2, and 3 represent pitch motion about the y axis, vertical motion along the z axis, and longitudinal motion along the x axis, respectively. The axis system has the origin fixed at the airplane's center of mass with the x axis oriented along the ground speed vector. Expanding C_m, C_L, and C_D plus adding an arbitrary pitch control variable, θ_C, to Equation 2 yields

$$\dot{q} = D_7 F_T + D_5 V_a^2 (C_{m_0} + C_{m_\alpha} \alpha' + C_{m_{\delta_E}} \delta_E + (D_4 C_{m_q}/V_a)q + (D_4 C_{m_{\dot\alpha}}/V_a)\dot\alpha') \tag{4}$$

$$\dot\gamma V = D_6 \sin(\delta_T + \alpha)F_T - D_2 \cos\gamma + D_1 V_a^2 (C_{L_0} + C_{L_\alpha}\alpha' + C_{L_{\delta_E}}\delta_E$$

$$+ (D_4 C_{L_q}/V_a)q + (D_4 C_{L_{\dot\alpha}}/V_a)\dot\alpha') \cos\delta - D_1 V_a^2 (C_{D_0} + C_{D_\alpha}\alpha'$$

$$+ C_{D_{\alpha^2}}\alpha'^2) \sin\delta - \theta_C \tag{5}$$

$$\dot V = D_6 \cos(\delta_T + \alpha)F_T - D_2 \sin\gamma - D_1 V_a^2 (C_{L_0} + C_{L_\alpha}\alpha' + C_{L_{\delta_E}}\delta_E$$

$$+ (D_4 C_{L_q}/V_a)q + (D_4 C_{L_{\dot\alpha}}/V_a)\dot\alpha') \sin\delta - D_1 V_a^2 (C_{D_0} + C_{D_\alpha}\alpha' + C_{D_{\alpha^2}}\alpha'^2)$$

$$\times \cos\delta \tag{6}$$

Collecting coefficents of F_T, α', and δ_E in the three equations and setting all time derivatives to zero

$$
\begin{bmatrix}
D_7 & V_a^2 D_5 C_{m_\alpha} & D_5 V_a^2 C_{m_{\delta_E}} \\[2ex]
D_6 \sin(\delta_T + \alpha) & -V_a^2(D_1 C_{D_\alpha} + D_1 C_{D_{\alpha 2}}\alpha')\sin\delta + D_1 C_{L_\alpha} V_a^2 \cos\delta & D_1 V_a^2 C_{L_{\delta_E}} \cos\delta \\[2ex]
D_6 \cos(\delta_T + \alpha) & -V_a^2(D_1 C_{D_\alpha} + D_1 C_{D_{\alpha 2}}\alpha')\cos\delta - D_1 C_{L_\alpha} V_a^2 \sin\delta & -D_1 V_a^2 C_{L_{\delta_E}} \sin\delta
\end{bmatrix}
\begin{Bmatrix} F_T \\[2ex] \alpha' \\[2ex] \delta_E \end{Bmatrix}
\tag{7}
$$

Next, separating the remaining terms of the three equations, gives

$$
\left\{ V_a \ \frac{\dot z}{V} \ \frac{\dot x}{V} \ \theta_C \right\}
\begin{Bmatrix}
-(D_5 C_{m_0} V_a + D_5 D_4 C_{m_q} q + D_5 D_4 C_{m_{\dot\alpha}}\dot\alpha') \\[2ex]
0 \\[1ex]
0 \\[1ex]
0 \\[2ex]
-(D_1 C_{L_0} V_a + D_1 D_4 C_{L_q} q + D_1 D_4 C_{L_{\dot\alpha}}\dot\alpha')\cos\delta + D_1 C_{D_0} V_a \sin\delta \\[2ex]
0 \\[1ex]
D_2 \\[1ex]
1 \\[2ex]
(D_1 C_{L_0} V_a + D_1 D_4 C_{L_q} q + D_1 D_4 C_{L_{\dot\alpha}}\dot\alpha')\sin\delta + D_1 C_{D_0} V_a \cos\delta \\[2ex]
-D_2 \\[1ex]
0 \\[1ex]
0
\end{Bmatrix}
\tag{8}
$$

81

For computational convenience and clarity, we write Equations 7 and 8 as

$$
\begin{pmatrix} G_1 & G_8 V_a^2 & G_9 V_a^2 \\ G_7 & G_5 V_a^2 & G_6 V_a^2 \\ G_4 & G_2 V_a^2 & G_3 V_a^2 \end{pmatrix} \begin{pmatrix} F_T \\ \alpha' \\ \delta_E \end{pmatrix} = \begin{pmatrix} V_a & \dfrac{\dot{z}}{V} & \dfrac{\dot{x}}{V} & \theta_C \end{pmatrix} \begin{pmatrix} -G_{12} & -G_{11} & G_{10} \\ 0 & 0 & -D_2 \\ 0 & D_2 & 0 \\ 0 & 1 & 0 \end{pmatrix} \qquad (9)
$$

To solve for F_T and δ_E, we take the inverse of the 3x3 matrix on the left-hand side of Equation 9 which is

$$
\frac{1}{DET} \begin{pmatrix} (G_5 G_3 - G_2 G_6) V_a^4 & -(G_8 G_3 - G_2 G_9) V_a^4 & (G_8 G_6 - G_5 G_9) V_a^4 \\ -(G_7 G_3 - G_4 G_6) V_a^2 & (G_1 G_3 - G_4 G_9) V_a^2 & -(G_1 G_6 - G_7 G_9) V_a^2 \\ (G_7 G_2 - G_4 G_5) V_a^2 & -(G_1 G_2 - G_4 G_8) V_a^2 & (G_1 G_5 - G_7 G_8) V_a^2 \end{pmatrix} \qquad (10)
$$

where the determinant, DET, is equal to

$$
(G_1 G_5 G_3 + G_8 G_6 G_4 + G_9 G_7 G_2 - G_4 G_5 G_9 - G_2 G_6 G_1 - G_3 G_7 G_8) V_a^4
$$

$$
= [G_2 (G_9 G_7 - G_6 G_1) + G_3 (G_1 G_5 - G_7 G_8) + G_4 (G_6 G_8 - G_5 G_9)] V_a^4
$$

$$
= -(G_2 H_1 - G_3 H_2 + G_4 H_3) V_a^4
$$

$$
= -(H_4) V_a^4
$$

$$
= -(H_5) V_a^2
$$

Multiplying both sides of Equation 9 by Equation 10 yields

$$
\begin{pmatrix} F_T \\ \alpha' \\ \delta_E \end{pmatrix} = \begin{pmatrix} H_{11} & -H_{10} & H_9 \\ --- & --- & --- \\ -H_8 & H_7 & -H_6 \end{pmatrix} \begin{pmatrix} -G_{12} & 0 & 0 & 0 \\ -G_{11} & 0 & D_2 & 1 \\ G_{10} & -D_2 & 0 & 0 \end{pmatrix} \begin{pmatrix} V_a \\ \dot{z}/V \\ \dot{x}/V \\ \theta_C \end{pmatrix} \qquad (11)
$$

Since we are solving for F_T and δ_E, the terms of the second row of the inverse corresponding to α' were not derived. Solving for F_T, and δ_E gives

82

$$F_T = K_{T1}V_a + K_{T2}\frac{\dot{z}}{V} + K_{T3}\frac{\dot{x}}{V} + K_{T4}\,\theta_C \qquad (12)$$

$$\delta_E = K_{D1}V_a + K_{D2}\frac{\dot{z}}{V} + K_{D3}\frac{\dot{x}}{V} + K_{D4}\,\theta_C \qquad (13)$$

where

$$\begin{pmatrix} K_{T1} \\ K_{T2} \\ K_{T3} \\ K_{T4} \end{pmatrix}' = \begin{pmatrix} -H_{11}G_{12} + H_{10}G_{11} + H_9G_{10} \\ -H_9D_2 \\ -H_{10}D_2 \\ -H_{10} \end{pmatrix}' \qquad (14)$$

and

$$\begin{pmatrix} K_{D1} \\ K_{D2} \\ K_{D3} \\ K_{D4} \end{pmatrix}' = \begin{pmatrix} H_8G_{12} - H_7G_{11} - H_6G_{10} \\ H_6D_2 \\ H_7D_2 \\ H_7 \end{pmatrix}' \qquad (15)$$

Equations for G_i, H_j, D_k, and C_n appear in detail in the following section.

Equation Form of G_i, H_j, D_k, and C_n

$$G_1 = D_7$$

$$G_2 = -(C_1 + C_2\alpha')\cos\delta - C_3\sin\delta$$

$$G_3 = -C_4\sin\delta$$

$$G_4 = D_6\cos(\delta_T + \alpha)$$

$$G_5 = C_3\cos\delta - (C_1 + C_2\alpha')\sin\delta$$

$$G_6 = C_4\cos\delta$$

$$G_7 = D_6\sin(\delta_T + \alpha)$$

$G_8 = C_5$

$G_9 = C_6$

$G_{10} = C_7 V_a \cos \delta + (C_8 V_a + C_9 q + C_{10} \dot{\alpha}') \sin \delta$

$G_{11} = (C_8 V_a + C_9 q + C_{10} \dot{\alpha}') \cos \delta - C_7 V_a \sin \delta$

$G_{12} = C_{11} V_a + C_{12} q + C_{13} \dot{\alpha}'$

$H_1 = G_6 G_1 - G_7 G_9$

$H_2 = G_5 G_1 - G_7 G_8$

$H_3 = G_5 G_9 - G_6 G_8$

$H_4 = G_2 H_1 - G_3 H_2 + G_4 H_3$

$H_5 = V_a^2 H_4$

$H_6 = H_2 / H_5$

$H_7 = (G_2 G_1 - G_4 G_8) / H_5$

$H_8 = (G_2 G_7 - G_4 G_5) / H_5$

$H_9 = H_3 / H_4$

$H_{10} = (G_2 G_9 - G_3 G_8) / H_4$

$H_{11} = (G_2 G_6 - G_3 G_5) / H_4$

$D_1 = (\rho/2)(SHA/m)$

$D_2 = (gHA/V_a^2)$

$D_3 = (HA^2/V_a^2)$

$D_4 = (\bar{c}/2HA)$

$D_5 = (\rho/2)(S\bar{c}HA^2/g\ I_{yy})$

$D_6 = (gHA/mV_a^2)$

$D_7 = (L_T D_3 / I_{yy})$

The following are the "C" coefficients used in variable gain computations of F_T and δ_E:

$$C_1 = D_1 C_{D_\alpha}$$

$$C_2 = D_1 C_{D_{\alpha^2}}$$

$$C_3 = D_1 C_{L_\alpha}$$

$$C_4 = D_1 C_{L_{\delta_E}}$$

$$C_5 = D_5 C_{m_\alpha}$$

$$C_6 = D_5 C_{m_{\delta_E}}$$

$$C_7 = D_1 C_{D_0}$$

$$C_8 = D_1 C_{L_0}$$

$$C_9 = D_1 D_4 C_{L_q}$$

$$C_{10} = D_1 D_4 C_{L_{\dot\alpha}}$$

$$C_{11} = D_5 C_{m_0}$$

$$C_{12} = D_5 D_4 C_{m_q}$$

$$C_{13} = D_5 D_4 C_{m_{\dot\alpha}},$$

APPENDIX B

CHARACTERISTICS OF AIRCRAFT USED IN
NUMERICAL FLIGHT SIMULATIONS*

	Boeing 727	Queen Air
Reference (scale) altitude HA (m)	91.4	91.4
Initial approach airspeed V_{a_0} (m/s)	71.9	56.4
Initial flight path angle γ (deg)	-3.0	-3.0
Aircraft mass (kg)	63,945.6	3,469.2
Moment of inertia I_{yy} (kg-m^2)	6.1×10^6	7.8×10^3
Moment arm of thrust vector L_T(m)	0.0	0.0
Angle between F_T and fuselage reference line (deg)	0.0	0.0
Chord length $\bar{c}$ (m)	5.0	1.8
Wing area S (m^2)	145.0	27.3

	Boeing 727	Queen Air**
C_{L_o}	1.360	0.639
C_{L_α}	5.04/rad	5.28/rad
$C_{L_{\delta_E}}$	0.007/deg	0.007/deg
C_{L_q}	9.3/rad	2.9/rad

---

*Courtesy of E. F. Blick, Professor of Aerospace Engineering, Department of Engineering, University of Oklahoma, Norman, Oklahoma.

**Based on approach speed of 62 m/s.

$C_{L_{\dot{\alpha}}}$	6.6	1.08
C_{D_O}	0.139	0.08
$C_{D_{\alpha}}$	1.245/rad	0.33/rad
$C_{D_{\alpha^2}}$	0.0/rad^2	0.0/rad^2
C_{m_O}	0.0	0.0
$C_{m_{\alpha}}$	-1.47/rad	-1.0/rad
$C_{m_{\delta_E}}$	-0.025/deg	-0.025/deg
C_{m_q}	-29.5/rad	-8.7/rad
$C_{m_{\dot{\alpha}}}$	-1.77/rad	-3.24/rad

1. REPORT NO. NASA CR-3342	2. GOVERNMENT ACCESSION NO.	3. RECIPIENT'S CATALOG NO.	
4. TITLE AND SUBTITLE Pilot-Aircraft System Response to Wind Shear		5. REPORT DATE November 1980	
		6. PERFORMING ORGANIZATION CODE	
7. AUTHOR(S) Barry S. Turkel and Walter Frost		8. PERFORMING ORGANIZATION REPORT #	
9. PERFORMING ORGANIZATION NAME AND ADDRESS FWG Associates, Inc. R.R. 2, Box 271-A Tullahoma, TN 37388		10. WORK UNIT NO. M-307	
		11. CONTRACT OR GRANT NO. NAS8-33458	
12. SPONSORING AGENCY NAME AND ADDRESS National Aeronautics and Space Administration Washington, D.C. 20546		13. TYPE OF REPORT & PERIOD COVERED Contractor Report	
		14. SPONSORING AGENCY CODE	

16. ABSTRACT

The nonlinear aircraft motion and automatic control computer model of Frost and Reddy has been expanded to incorporate the human pilot into simulations of aircraft response to wind shear. The human pilot is described by a constant gains lag filter. In addition, two runs are carried out using pilot transfer functions from the experimental data of Adams and Bergeron. Fixed-stick, autopilot, and manned computer simulations are made with an aircraft having characteristics of a Queen Air (small commuter-type aircraft) flown through longitudinal winds measured by a Doppler radar beamed along the glide slope during the SESAME '79 experiments in Oklahoma. Simulations are also made flying an aircraft characteristic of a Boeing 727 through sinusoidal head wind and tail wind shears at the phugoid frequency to evaluate the response of manned aircraft in thunderstorm wind environments.

17. KEY WORDS Wind Shear Flight Simulation	18. DISTRIBUTION STATEMENT Unclassified – Unlimited STAR Category 47		
19. SECURITY CLASSIF. (of this report) Unclassified	20. SECURITY CLASSIF. (of this page) Unclassified	21. NO. OF PAGES 106	22. PRICE A06

MSFC - Form 3292 (Rev. December 1972)

For sale by National Technical Information Service, Springfield, Virginia 22161